Soft Matter

REVIEW

View Article Online
View Journal | View Issue

Polyelectrolyte adsorption, interparticle forces, and colloidal aggregation

Cite this: *Soft Matter*, 2014, **10**, 2479

Istvan Szilagyi, Gregor Trefalt, Alberto Tiraferri, Plinio Maroni and Michal Borkovec*

This review summarizes the current understanding of adsorption of polyelectrolytes to oppositely charged solid substrates, the resulting interaction forces between such substrates, and consequences for colloidal particle aggregation. The following conclusions can be reached based on experimental findings. Polyelectrolytes adsorb to oppositely charged solid substrates irreversibly up to saturation, whereby loose and thin monolayers are formed. The adsorbed polyelectrolytes normally carry a substantial amount of charge, which leads to a charge reversal. Frequently, the adsorbed films are laterally heterogeneous. With increasing salt levels, the adsorbed mass increases leading to thicker and more homogeneous films. Interaction forces between surfaces coated with saturated polyelectrolyte layers are governed at low salt levels by repulsive electric double layer interactions, and particle suspensions are stable under these conditions. At appropriately high salt levels, the forces become attractive, principally due to van der Waals interactions, but eventually also through other forces, and suspensions become unstable. This situation can be rationalized with the classical theory of Derjaguin, Landau, Verwey, and Overbeek (DLVO). Due to the irreversible nature of the adsorption process, stable unsaturated layers form in colloidal particle suspensions at lower polyelectrolyte doses. An unsaturated polyelectrolyte layer can neutralize the overall particle surface charge. Away from the charge reversal point, electric double layer forces are dominant and particle suspensions are stable. As the charge reversal point is approached, attractive van der Waals forces become important, and particle suspensions become unstable. This behaviour is again in line with the DLVO theory, which may even apply quantitatively, provided the polyelectrolyte films are sufficiently laterally homogeneous. For heterogeneous films, additional attractive patch–charge interactions may become important. Depletion interactions may also lead to attractive forces and suspension destabilization, but such interactions become important only at high polyelectrolyte concentrations.

Received 8th August 2013
Accepted 15th January 2014

DOI: 10.1039/c3sm52132j

www.rsc.org/softmatter

1 Introduction

Charged polymers or polyelectrolytes (PEs) are widely employed to modify properties of surfaces or of colloidal particle suspensions. They are industrially used in water purification,

Department of Inorganic and Analytical Chemistry, University of Geneva, Sciences II, Quai Ernest-Ansermet 30, 1205 Geneva, Switzerland. E-mail: michal.borkovec@unige.ch

Istvan Szilagyi is a senior lecturer at the University of Geneva since 2009. He got his PhD in inorganic chemistry at the University of Szeged, Hungary, in 2006. He was then a postdoctoral researcher at the Murdoch University, Perth, Australia. His research focuses on inorganic and colloid chemistry and the development of novel functional materials.

Gregor Trefalt is a postdoctoral researcher at the University of Geneva. He studied chemistry at the University of Ljubljana, Slovenia. He stayed in Ljubljana to obtain his PhD in 2012 at Jožef Stefan Institute to carry out research in the area of colloidal processing of ceramic materials. He now focuses on colloidal interactions, particle aggregation, and light scattering.

papermaking, mineral separation, or to control flow properties of particle slurries.[1–6] Emerging industrial applications of PEs include, for example, stabilization of metallic iron particles for environmental remediation, use as additives in the chemical–mechanical polishing process, or in biomedical applications.[7–11] PEs are further employed to create protective or functional surface coatings, whereby important approaches include adsorption of PE monolayers,[7,12–14] fabrication of multilayers of oppositely charged PEs,[13,15–18] or the preparation of PE brushes by grafting or by adsorption of block copolymers.[19–21] Such coatings may be used to control surface properties, including wetting, lubrication, adhesion, or biological resistance.[22,23] Certain PEs offer the possibility to tune these properties through external stimuli, such as temperature or solution composition.[24,25]

PEs interact strongly with solid substrates, and in turn, they may substantially alter the respective surface characteristics. Thereby, the interaction forces between such surfaces can be modified, and as a consequence, properties of particle suspensions can be controlled. Understanding of the relationship between PE adsorption, particle interactions, and the stability of the resulting suspensions is critical for further development of functional PE additives. The present review attempts to draw a systematic picture of these processes for the relevant situation when PEs adsorb onto oppositely charged solid substrates.

PE adsorption to solid substrates and the resulting charging behaviour were investigated by numerous experimental techniques. Planar substrates were probed with optical reflectivity, ellipsometry, quartz crystal microbalance, and streaming potential techniques,[26–28] while particle suspensions were characterized by means of classical batch depletion techniques, light, X-ray and neutron scattering, and electrophoresis.[29–32] This review will focus on linear or branched homopolymers, including dendrimers, in monovalent electrolyte solutions. We will further investigate properties of PE films in the same electrolyte solution as that used for the adsorption process and discuss the influence of salt concentration and effects of charge densities of the PEs and of the substrate. PE adsorption will be mainly interpreted in terms of the random sequential adsorption (RSA) model and its variants,[33,34] while the self-consistent field approach and computer simulation studies will be addressed only briefly.[35–41]

Adsorbed PEs modify interaction forces acting between substrates, and for this reason, they are frequently used as additives to control the stability of colloidal suspensions or to tune their rheological properties.[1–4,7] The resulting interaction forces between surfaces or particles in the presence of PEs were investigated with the surface forces apparatus (SFA),[42,43] total internal reflection microscope,[44–46] or the colloidal probe technique based on the atomic force microscope (AFM).[47,48] Particle aggregation phenomena were investigated with turbidity measurements, time-resolved light scattering, or rheology.[4,49–51] We only focus on interactions in symmetric systems involving the same type of interfaces or particles, and correspondingly on homoaggregation processes.

An interpretation of the underlying mechanisms of the adsorption process, interaction forces, and particle aggregation will be put forward. We explore to what extent interaction forces can be rationalized in terms of the classical theory of Derjaguin, Landau, Verwey, and Overbeek (DLVO).[52–54] The role of specific

Alberto Tiraferri is a Marie Curie postdoctoral fellow at the University of Geneva. He studied environmental engineering at the Politecnico di Torino, Italy, and received his PhD in 2012 at Yale University, New Haven, USA, in the area of membrane-based separation processes for water treatment. His current project explores the adsorption of macromolecules to surfaces and implication of these processes to membrane fouling and environmental remediation.

Plinio Maroni works as a senior scientist at the University of Geneva. He studied physics at the University of Pisa, Italy and he got his PhD in 2005 at the Swiss Federal Institute of Technology, Lausanne, in the area of molecular reactivity of molecules adsorbed on surfaces. His current research interests center around surface spectroscopy, surface sensitive optical and acoustic techniques, and local probe microscopy.

Michal Borkovec is a full professor of chemistry at the University of Geneva and a member of the Swiss National Research Council. He received his PhD in 1986 at Columbia University, New York, USA, and then worked as a lecturer at the Swiss Federal Institute of Technology, Zürich. Later, he became an associate professor at Clarkson University, Potsdam, USA, and in 2001 he accepted his current position at Geneva. His research interests include physical chemistry of colloids, interfaces, and polyelectrolytes.

forces induced by PEs, in particular, steric, bridging, and depletion interactions will be equally discussed.[54] The relevance of these forces in controlling the suspension stability in the presence of PEs was proposed early on.[55] We will further discuss the patch–charge interactions resulting from the lateral heterogeneity of the adsorbed PE layers.[56] Simple models will be used to clarify the mechanisms of the interactions involved.

There are various important topics involving PE adsorption that will not be addressed in this review. We shall skip the interesting aspects related to adsorption of comb polymers, such as bottlebrush and dendronized polymers[57–59] or copolymers, such as block copolymers and proteins.[60–66] The response of adsorbed PE films when exposed to solutions of variable compositions or containing multivalent ions will not be addressed either.[67–75] We will not discuss mixed adsorbed PE films, which are especially important for multilayers prepared by the layer-by-layer deposition process,[13,15–18,24,76,77] as well as the adsorption of neutral polymers or PEs with the same sign of charge as the substrate.[35,73,75,78] Neither the adsorption of PEs to interfaces under applied external electric potential, nor to instable or fluid interfaces (*e.g.*, air–water and oil–water) will be addressed.[79–82] We also skip the discussion of interaction forces in asymmetric systems involving different types of surfaces, heteroaggregation, particle deposition, or growth of particle–PE multilayers.[83–87] Finally, we make no attempt to provide a detailed review of the numerous theoretical developments and computer simulations addressing PE adsorption and the resulting interaction forces. For these topics, we refer the interested reader to the appropriate literature.[36–38,88]

The present review is organized as follows. Section 2 summarizes the current understanding of the PE adsorption phenomena and the underlying charging process, whereby planar substrates as well as colloidal particles are discussed. Interaction forces between the same type of interfaces, either involving planar substrates, colloidal particles, or both, are addressed in Section 3. Particle aggregation phenomena involving the same type of particles are addressed in Section 4, whereby the main focus is on early stages of the homoaggregation process. An outlook highlighting open questions and possible research directions concludes the review.

2 Polyelectrolyte adsorption

This section focuses on adsorption of polyelectrolytes (PEs) to oppositely charged water–solid interfaces. These interfaces might be realized by means of a planar substrate or through the internal surface in a colloidal particle suspension. PEs normally have a linear architecture and some examples are summarized in Fig. 1. PEs can also be branched and corresponding examples include dendritic poly(amido amine) (PAMAM) or branched poly(ethylene imine) (BPEI). One refers to anionic and cationic PEs when they are negatively and positively charged, respectively. PEs with a permanent charge are called strong PEs, and they include sodium poly(styrene sulfonate) (PSS) and poly(diallyldimethyl ammonium) (PDDA). The charge of weak PEs varies with solution pH and ionic strength, and examples include poly(vinyl amine) (PVA), poly(L-lysine) (PLL), poly(acrylic acid) (PAA), linear poly(ethylene imine) (LPEI) or PAMAM. Their degree of ionization can be measured by potentiometric titrations and modelled with mean field or site binding models.[89] In monovalent electrolyte solutions, the gyration radius R_g of linear PEs obeys the classical scaling law[90]

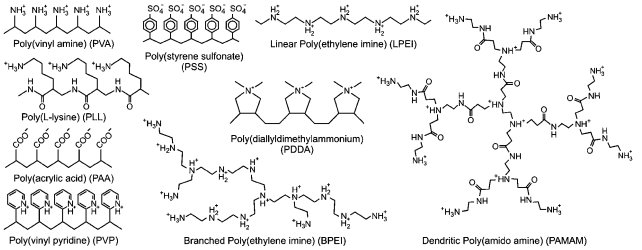

Fig. 1 Structural formulae of various fully ionized PEs discussed in this review. The names and acronyms refer to the ionized forms of the strong PEs, while to the neutral forms of the weak PEs.

$$R_g \propto M^{\alpha} \quad (1)$$

where M is the molecular mass and α is the Flory exponent in the range 0.5–0.6. The hydrodynamic radius that is related to the diffusion coefficient of the PE chain is typically a factor of 1.5–2.0 smaller.[90] Adsorption of PEs will be discussed in the following.

2.1 Irreversible nature of the adsorption process

Highly charged PEs adsorb strongly to oppositely charged interfaces. This affinity is primarily caused by attractive electrostatic forces acting between the oppositely charged PE and substrate. Since the PE backbone is hydrophobic, however, attractive van der Waals and hydration forces are important as well. This subsection will compare adsorption to planar substrates and in colloidal suspensions and rationalize this process with simple models.

Adsorption of PEs to planar substrates. Numerous optical techniques are available to study the adsorption of PEs to planar solid substrates in real time.[27,79,91–94] Let us illustrate the adsorption process of PEs to oppositely charged substrates with reflectivity experiments as displayed in Fig. 2a, which allows monitoring of the change in the adsorbed mass per unit area. The example shown refers to strong cationic PDDA of molecular mass of about 450 kg mol^{-1} adsorbing to a negatively charged silica substrate.[91] The substrate is initially rinsed with a pure electrolyte solution adjusted to pH 4.0, and then the solution is changed to a PE solution in the same electrolyte and of the same pH. The adsorbed mass of the PE increases linearly with time at first. This increase reflects the rapid adsorption of the PE to the surface. Later, the adsorbed mass reaches a plateau. This plateau indicates that the PE film is saturated, and in spite of the presence of PE in the solution, no further adsorption occurs. When the surface is rinsed with the pure electrolyte solution, no desorption is observed. This feature suggests that the adsorption process is irreversible. If this process would be reversible, the PE would desorb from the surface, and the desorption could

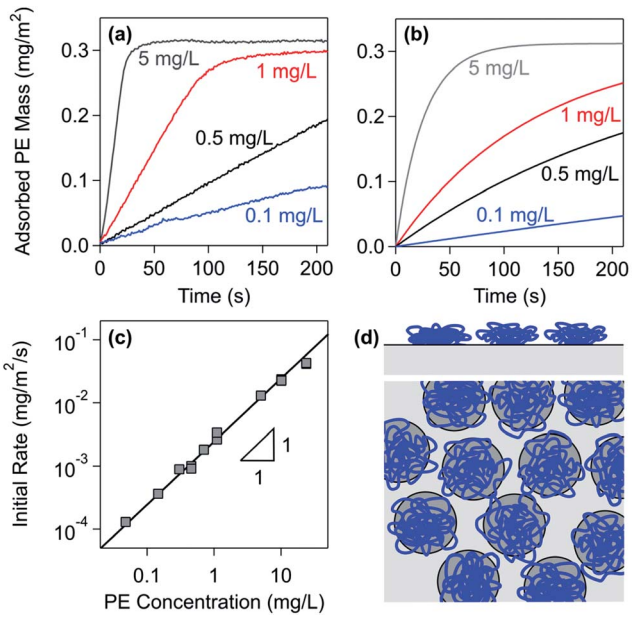

Fig. 2 Adsorption kinetics of PDDA to the silica surface in a solution of 50 mM monovalent salt at pH 4. (a) Measurements with optical reflectivity at different PE concentrations.[91] (b) Results of the simple irreversible adsorption model with the Langmuir blocking function. (c) Initial adsorption rate *versus* different PE concentrations. (d) Graphical illustration of the RSA model.

be evidenced in the reflectivity trace. The fact that adsorbed PE layers do not desorb in the PE-free electrolyte solution has been demonstrated in numerous systems.[27,34,82,91,95–98]

Partial desorption could be only demonstrated for PEs in special circumstances, for example, for PEs of very low molecular mass, typically below 10 kg mol^{-1}.[27,95] Desorption of PEs of higher molecular mass has been reported to be induced by changes in the solution composition or by exchange with other PEs.[27,58,99] However, the adsorption process is irreversible provided the composition of the electrolyte solution is not changed during the experiment.

With increasing concentration of the PE, the initial adsorption rate increases.[91] The rate law can be identified by plotting the initial rate *versus* the PE concentration as shown in Fig. 2c. Since this rate is proportional to the PE concentration, the adsorption process follows a first-order rate law in the PE concentration. Similar dependencies were observed with other PEs.[34,97,100]

Converting the data shown in Fig. 2c into the adsorbed number density, one finds an adsorption rate coefficient of $k_a = 2.5 \times 10^{-6}$ m s^{-1}. This rate coefficient can also be calculated from the cell geometry by assuming laminar flow and perfect sink conditions.[34,101] Based on the known flow rate and the hydrodynamic radius of PDDA of about 26 nm as estimated from light scattering experiments,[90,102] the perfect sink model predicts a rate coefficient of $k_a = 4.9 \times 10^{-6}$ m s^{-1}. This value is only about a factor two larger than the one observed experimentally. The remaining discrepancy could be related to forces acting between the PE and the substrate and to hydrodynamic interactions. A similar agreement between experimental and calculated adsorption rate coefficients was reported in other PE systems.[34,97,100]

The plateau value is independent of the PE concentration to good approximation. However, this value may increase with increasing PE concentration somewhat. This increase can be rationalized by the finite relaxation time of the polymer chains.[28,76,91] With increasing PE concentration, the lateral relaxation of the individual adsorbing PEs is increasingly hindered by the rapidly arriving neighbouring PEs. A similar relaxation mechanism was also suggested to be present for protein adsorption.[103]

Classical RSA model. This model describes irreversible adsorption processes of colloidal particles, proteins, and PEs.[104–106] The particles are modeled as circular disks, and they are assumed to adsorb to a planar surface sequentially at random locations. Such a disk can only adsorb on an empty surface and an overlap with a previously deposited disk is not allowed; see Fig. 2d. The maximum coverage or the so-called jamming limit is[104,105]

$$\theta_{jam} \simeq 0.55 \tag{2}$$

which is substantially smaller than the regular hexagonal packing with a coverage of 0.91. The surface coverage θ can be related to the number density of adsorbed PE molecules Γ per unit area by

$$\theta = \pi a^2 \Gamma \tag{3}$$

where a is the disk radius, which is comparable to the gyration radius of the PE. The kinetics of the adsorption process can be approximated by relating the rate of change of the adsorbed number density with time t to the number concentration c of the PE in solution as

$$\frac{d\Gamma}{dt} = k_a c B(\Gamma) \tag{4}$$

where k_a is the adsorption rate coefficient of the PE and $B(\Gamma)$ is the blocking (or available surface area) function. The Langmuir adsorption model suggests that

$$B(\Gamma) = \begin{cases} 1 - \Gamma/\Gamma_0 & \text{for } \Gamma < \Gamma_0 \\ 0 & \text{for } \Gamma \geq \Gamma_0 \end{cases} \tag{5}$$

where Γ_0 is the adsorbed number density at saturation, which corresponds to the jamming limit within the RSA model. The predictions of this kinetic model are shown in Fig. 2b. The adsorbed mass per unit area is obtained by multiplying the adsorbed number density Γ with the mass of the PE. The model results agree with the experiment semi-quantitatively.

However, the model predicts a too gradual transition from the initial stages to saturation. An analysis of the RSA model leads to a blocking function, which suggests an even slower approach to saturation. Alternative blocking functions have been proposed to remedy this problem.[66,105,106] However, they were mainly used to describe irreversible adsorption of particles and proteins and have not been applied to model PE adsorption so far.

Adsorption of PEs to colloidal particles. When PEs are dissolved in a suspension of colloidal particles, they will also adsorb to their surface irreversibly. In this situation, one should distinguish two cases as illustrated in Fig. 3. When the total PE concentration is high, the PEs will adsorb to the particle surface until a saturated layer is formed. The excess PE will remain dissolved in solution. When the total PE concentration is low, the PE will adsorb to the particle surface until no PE is left in solution. In this case, we refer to an unsaturated layer. When performing such experiments in colloidal suspensions, larger concentration gradients during mixing must be avoided, otherwise the PE may distribute among the particles unevenly.

The irreversible nature of the adsorption can be confirmed experimentally with batch adsorption experiments as well.[31,107] Fig. 3c shows results of adsorption of dendritic PAMAM to sulfate latex particles, where the adsorbed amount was obtained by counting the adsorbed single molecules with the AFM.[108] The adsorbed mass is plotted *versus* the PE dose, which reflects the mass of PE relative to the mass of the particles (mg g^{-1}).

At high PE doses, the adsorbed mass is constant due to saturation. The fact that the total adsorbed mass is independent of the solution concentrations was also experimentally confirmed with PVA and PDDA adsorbing to latex particles.[30,31,107] At low doses, the entire quantity of PE added is adsorbed, but is insufficient to achieve saturation, meaning that the plateau is not reached. The PE dose can be also expressed as the mass of the PE per unit particle surface area (mg m^{-2}). These units are useful in the unsaturated regime, where the dose simply reflects the adsorbed mass. The fact that adsorption in the unsaturated regime is quantitative can be also demonstrated by electrophoresis, and this technique will be discussed in Section 2.3.

Deviations from this idealized picture occur due to the kinetics of the adsorption process. This process can be particularly slow when the PE concentration is close to the one needed to reach saturation. The simple model summarized in eqn (4) and (5) can be also used to model adsorption in suspensions, and the corresponding results are illustrated in Fig. 3d. When the adsorption time is too short such that adsorption cannot be completed, the plot of the adsorbed mass *versus* the PE concentration will be rounded. Such dependencies might be wrongly interpreted by an equilibrium adsorption isotherm.

When a substrate is continuously flushed with PE solution in a flow-through cell, one always obtains a saturated layer due to a sufficient supply of PEs. Unsaturated layers can be formed in a flow-through cell too. In that case, however, the PE feed solution must be changed to a pure electrolyte solution before the saturation plateau is reached.

2.2 Properties of adsorbed polyelectrolyte layers

Let us now discuss the main characteristics of saturated PE layers, particularly, the adsorbed mass, their thickness, water content, and lateral heterogeneity. Not much is known concerning the unsaturated layers, but we will also comment on those. The RSA model will be further generalized to introduce effects of electrostatic interactions.

Absorbed mass. Fig. 2a illustrates that the adsorbed mass at saturation for PDDA on silica in 50 mM salt solution is about 0.3 mg m^{-2}. These are small amounts, since an atomic monolayer corresponds to about 1–2 mg m^{-2}. Let us rationalize with the RSA model on why such a small amount corresponds already to saturation. Taking the hydrodynamic radius of about 26 nm for PDDA[91] and the maximum coverage given by eqn (2), one finds an adsorbed mass of 0.1 mg m^{-2}. The RSA model provides indeed a reasonable estimate, which supports the picture that the adsorbed film corresponds to a monolayer of adsorbed PE chains. In general, the mass adsorbed for saturated PE layers adsorbed to oppositely charged substrates can be even lower and typically is 0.01–1 mg m^{-2}.[34,91,98,109–112]

The mass of adsorbed PE depends on several factors related to the characteristics of the PE, those of the substrates, and the solution composition. Here, we discuss effects of the molecular mass, salt concentration, as well as the influence of the charge density of the PE and the substrate. These findings will be then explained in terms of a modified RSA model that includes electrostatic interactions between adsorbed molecules.

The adsorbed mass at saturation depends only weakly on the molecular mass for linear PEs.[28,32] This observation can be also rationalized with the RSA model. Based on eqn (1) and (3), this model suggests that the adsorbed number density scales as

$$\Gamma \propto M^{-2\alpha} \tag{6}$$

with the molecular mass M. From this relationship one finds that the adsorbed mass scales as $\propto M^{1-2\alpha}$. For typical values of the exponent α, this relationship leads to an extremely weak dependence. On the other hand, for dendritic or branched PEs, the adsorbed mass increases with the molecular mass more

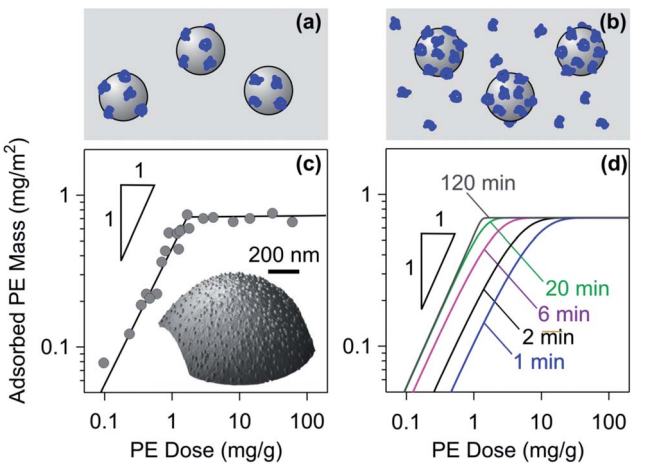

Fig. 3 Adsorption of PEs in a colloidal suspension of oppositely charged particles. Schematic representation of (a) the unsaturated layer that depletes the solution of the free PE and (b) the saturated layer with excess PE in solution. (c) Overnight adsorption of dendritic PAMAM of 935 kg mol^{-1} to sulfate latex particles of diameter 3.1 μm in a colloidal suspension of pH 4.0 without salt added. The adsorbed amount was obtained by counting from AFM images shown in the inset.[108] The solid line represents the expected adsorbed amount given the saturation value. (d) Representative results with the kinetic RSA model where the effect of finite adsorption time is indicated.

strongly, since the exponent α is much smaller than that for linear PEs.[34,95,113]

The adsorbed mass normally increases with increasing concentration of the added monovalent electrolyte. Fig. 4 illustrates this trend for various PEs and substrates. This increase has been observed for a wide range of cationic and anionic PEs adsorbed on oppositely charged substrates, and typically results in an increase by a factor 2–4 when the salt concentration is increased by 4 orders of magnitude.[28,32,34,91,97,98,110,112,114–116] This salt dependence only reverses for very weakly charged PEs and high salt concentrations, whereby the adsorbed mass goes through a maximum, and finally decreases.[97,98,117–119]

Trends concerning the variation of the charge densities are less clearly established. The charge density of PEs can be varied by studying copolymers involving charged and neutral monomers, but other properties of the PEs may change at the same time (*e.g.*, hydrophobicity).[31,111] The charge density of the substrates has been sometimes varied by investigating different oxides, but other characteristics of these substrates are altered in this fashion as well.[26,27] A good way to tune the charge density of PEs and of the substrates is through weak ionizable groups and the respective pH adjustments. Nevertheless, the charges of the isolated components may not correspond to the ones in the adsorbed state, since ionization may occur upon adsorption.[117,120,121] The adsorbed mass normally increases with increasing charge density of the substrate and with decreasing charge density of the PE.[29,34,91,111] With decreasing PE charge density, the adsorbed mass may go through a maximum at very low charge densities.[29,111,119,122]

Electrostatic RSA model. The increase of the adsorbed mass with the salt concentration can be understood by considering the repulsion of the electric double layers formed around adsorbing PE coils. When the salt level is decreased, the repulsion becomes increasingly long ranged, which leads to saturation of the surface at lower adsorbed amounts.

This situation can be captured by a simple modification of the RSA model.[106,123,124] Since the adsorbing polymers repel each other due to overlapping electric double layers, one can model this phenomenon as an increase in the radius of the adsorbing disks to an effective radius a_{eff}, which now also includes the range of the repulsion of the surrounding diffuse layer. The situation is schematically depicted in Fig. 4d. The resulting surface coverage is now given by

$$\theta = \theta_{\mathrm{jam}} \left(\frac{a}{a_{\mathrm{eff}}} \right)^2 \tag{7}$$

The effective radius a_{eff} can be estimated by assuming that the interaction energy of two neighbouring PE chains will be comparable to the thermal energy, namely

$$u(2a_{\mathrm{eff}}) \simeq k_{\mathrm{B}}T \tag{8}$$

where $u(r)$ is the interaction potential between two adsorbing PEs at a center-to-center distance r and $k_{\mathrm{B}}T$ is the thermal energy with k_{B} being the Boltzmann constant and T being the absolute temperature. The screened Coulombic interaction can be used to model the interaction between two charged spheres in solution[106,123,124]

$$u(r) = k_{\mathrm{B}}T L_{\mathrm{B}} {Z_{\mathrm{eff}}}^2 \left(\frac{\mathrm{e}^{\kappa a}}{1+\kappa a} \right)^2 \frac{\mathrm{e}^{-\kappa r}}{r} \tag{9}$$

where Z_{eff} is the effective charge in units of the elementary charge q, and the Bjerrum length is abbreviated as

$$L_{\mathrm{B}} = \frac{q^2}{4\pi k_{\mathrm{B}} T \varepsilon_0 \varepsilon} \simeq 0.72 \text{ nm} \tag{10}$$

where ε_0 is the permittivity of vacuum and ε is the dielectric constant of the liquid. The Debye length κ^{-1} in a monovalent electrolyte is given by

$$\kappa^2 = 8\pi L_{\mathrm{B}} N_{\mathrm{A}} c_{\mathrm{S}} \text{ or } \kappa^{-1} \simeq \frac{0.30\,\mathrm{nm}}{\sqrt{c_{\mathrm{S}}}} \tag{11}$$

where c_{S} is the molar concentration of the electrolyte and N_{A} is the Avogadro's number. The numerical values refer to water at room temperature and the salt concentration is expressed in mol L^{-1}. For weakly charged objects, the effective charge Z_{eff} simply corresponds to the bare charge Z. For objects of higher charge, the effective charge will be lower than the bare charge due to adsorption of counterions. Poisson–Boltzmann theory suggests that the effective charge is constant for highly charged objects and is given by[124]

$$Z_{\mathrm{eff}} = \frac{a}{L_{\mathrm{B}}} (4\kappa a + 6) \tag{12}$$

The effective radius a_{eff} can be now estimated from eqn (8) and (9), and the adsorbed number density follows from eqn (3) and (7).

Results obtained from this modified RSA model are shown in Fig. 4a. One observes that this model predicts very similar dependencies to the ones observed for the adsorption of PDDA and dendritic PAMAM.[34,91] Fig. 4b shows a dimensionless representation of the surface coverage θ *versus* the screening parameter κa where the curves almost collapse on a master curve.[124,125] This model can qualitatively explain the characteristic increase of the adsorbed mass with decreasing charge density of the PE. In this case, decreasing the effective charge Z_{eff} will lead to smaller effective radii a_{eff} and therefore to larger adsorbed mass.

The RSA model can be further extended to rationalize the increase of the adsorbed mass with increasing charge density of the substrate.[34] At charged water–solid interfaces, electrical double layers form, and the diffuse layer contains a higher concentration of counterions than the one in the bulk. When two PE chains interact close to the interface, the higher concentration of counterions close to the interface will enhance the screening of the electrostatic interaction. Therefore, the electrostatic repulsion between the adsorbing chains will be weaker and result in a larger adsorbed mass. This effect can be included into the RSA model, and the modified model can explain the increase of the adsorbed amount of dendritic PAMAM with the solution pH quite well.[34] The more substantial adsorbed amounts of PAMAM compared to other PEs at very low salt concentrations shown in Fig. 4c can be probably rationalized through the same mechanism. The spirit of the electrostatic RSA model is similar to the treatment of the dilute 2-d

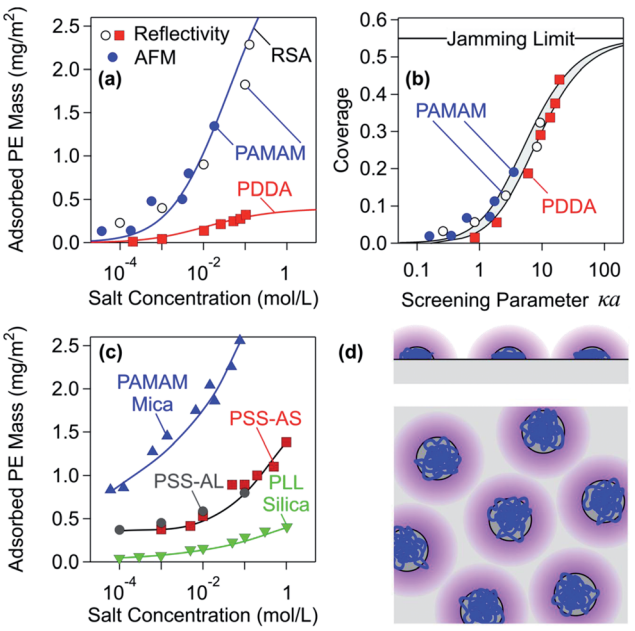

Fig. 4 Adsorbed mass of PEs on oppositely charged substrates *versus* salt concentration at saturation. (a) Adsorbed mass *versus* the salt concentration for dendritic PAMAM and linear PDDA on silica measured by reflectivity and AFM and comparison with the RSA model (solid lines).[34,91] (b) Dimensionless representation of the coverage θ *versus* screening parameter κa of the same data as shown in (a). The grey region corresponds to radii between 5 and 50 nm. (c) Further experimental results obtained with different substrates, namely mica, silica, amino-functionalized silica (AS), and amidine latex (AL). The solid lines serve as a guide to the eye. (d) Schematic representation of the electrostatic RSA model. The diffuse layer is indicated in purple.

Wigner regime, which makes the assumption that PEs adsorb individually and that their mutual interactions are dominated by diffuse layer repulsion.[126]

The RSA model is unable to predict the adsorption maximum that is observed for weakly charged PEs and high salt concentrations.[97,117,118] This maximum is related to the fact that PEs will not adsorb to oppositely charged substrates beyond a critical salt concentration threshold, if solely electrostatic forces are present.[39,119,127] At high salt levels, a weakly charged PE will be strongly screened. Therefore, attractive electrostatic forces acting between the PE and the substrate will be not sufficient to overcome the thermal motion, and the PE will no longer adsorb. Since the adsorbed amount increases with increasing salt levels, but vanishes above the salt threshold, a sharp maximum in the adsorbed amount results. In reality, however, additional attractive forces act between the PE chain and the substrate (*e.g.*, van der Waals and hydration). These non-electrostatic forces may be quite important, as evidenced by adsorption of neutral polymers. For PEs, however, the forces responsible for the adsorption weaken substantially beyond the salt threshold. Therefore, one observes a wider maximum with respect to the one expected from electrostatic forces alone. Under these conditions, the adsorption process may no longer be irreversible, and the simple RSA model is expected to fail. Alternative models capable of describing this situation are discussed below.

Morphology of adsorbed PE films. The electrostatic RSA model suggests that PE chains adsorb to the substrate individually. Since the spacing between the chains is mainly dictated by the electrostatic repulsion between the adsorbing chains, the film remains laterally heterogeneous. Moreover, strong attractive electrostatic forces acting between the adsorbing PE and the substrate are expected to flatten the adsorbed chains. Therefore, an adsorbed PE layer will be typically thin and laterally heterogeneous. For more weakly charged PEs, and especially at higher salt levels, more homogeneous layers may form. Let us now discuss the experimental evidence supporting these claims.

Fig. 5 summarizes layer thickness measurements of adsorbed PE films with two different techniques.[28,32] The first technique is based on dynamic light scattering (DLS) in a colloidal particle suspension, where the layer thickness is inferred from the difference between the hydrodynamic radii of the particles in the presence and in the absence of the PE; see Fig. 5a.[32,128] The second technique relies on a combination of optical reflectivity and quartz crystal microbalance measurements on planar substrates; see Fig. 5b.[28,129] Both techniques yield comparable results. PE layers adsorbed on oppositely charged substrates are extremely thin, merely a few nm. Considering the fact that the diameter of PE chains in solution typically is 20–100 nm, the PEs are strongly flattened in the adsorbed state. Based on these thickness measurements, one further concludes that these films are rather compact and contain only 20–60% of water.[28,32] At higher salt levels, however, these films become more swollen and porous. Few additional reports confirm that PE films adsorbed on oppositely charged substrates are very thin indeed.[18,111,130] One also finds that the layer thickness increases with increasing salt levels and with increasing molar mass, especially at high salt concentrations.[28] An increase in thickness was also reported with the decreasing charge of the PE, and this quantity also passes through a maximum at very low charge densities.[111]

While data shown in Fig. 5 clearly support the picture of flat adsorbed PE films, one observes that DLS measurements yield a larger thickness than the ones measured by the surface sensitive techniques. Moreover, the latter data suggest a more gradual swelling of the film. While the differences in the substrates used may lead to these differences, they might also be related to the two sub-layer structure of an adsorbed PE film.[94] The thickness of these sub-layers may vary upon solution conditions and lead to the different salt dependencies observed with the two different techniques. One should also realize that thickness measurements for such extremely thin films are difficult and prone to systematic errors. Some of the available results in the literature should be thus considered with caution.

The lateral heterogeneity of adsorbed PE films can be best confirmed by AFM imaging. Such non-uniformities are particularly pronounced for highly charged PEs and low salt levels. Fig. 6 shows such images of adsorbed PEs recorded in the dry state. Fig. 6a shows adsorbed dendritic PAMAM, and the individual molecules can be clearly distinguished. Note that this layer is saturated, and no further adsorption will occur, in spite

of the unoccupied surface in between individual molecules. This low coverage results from the strong electrostatic repulsion between the adsorbing dendrimers. The other images show linear PEs adsorbed to different substrates. Fig. 6b refers to a saturated layer of PSS on amidine latex particles.[131] Fig. 6c and d show unsaturated layers of poly(vinyl pyridine) (PVP) on mica.[132]

While such imaging techniques provide strong evidence that adsorbed PE layers are laterally heterogeneous, quantitative characterization of these heterogeneities is mostly lacking. Exceptions are layers formed with dendritic PAMAM, whereby the individual molecules can be resolved with AFM. They can be described as dilute monolayers and they feature a liquid-like order as indicated by a structural peak in the radial distribution function.[34,133] The statistical properties of individual adsorbed linear polyelectrolytes and of nucleic acids were successfully determined with the AFM.[74,132,134–136] However, little is known about the detailed structure of saturated layers of adsorbed linear polyelectrolytes and the characteristic distances involved. Direct force measurements have confirmed that adsorbed layers of dendritic PAMAM and linear PSS are heterogeneous.[107,131] These techniques have also demonstrated that similar layers formed with LPEI are homogeneous down to about 10 nm, but probably heterogeneous on smaller length scales.[48] Weakly charged hydrophobic PEs have been reported to form more homogeneous layers, resembling disordered lamellar phases.[74] Similar structures were also predicted on theoretical grounds and were also referred to as the semi-dilute 2-d Wigner regime.[88,126]

An alternative interpretation of the small layer thicknesses shown in Fig. 5 could be related to the lateral heterogeneity of the films. Typically, surface sensitive and scattering techniques yield a laterally averaged thickness, and dilute, heterogeneous layers would lead to a smaller thickness than the gyration radius of an individual PE even if the adsorption process did not lead to a deformation in the normal direction. However, height measurements of adsorbed dendritic PAMAM with the AFM indicate that even these molecules flatten substantially.[67,133] These highly branched molecules have rather compact structures, and therefore linear PEs will flatten much more.

Modeling of PE adsorption. The electrostatic RSA model was introduced above to understand some basic features of PE adsorption. However, various alternative models of the adsorption process of PEs to oppositely charged substrates have been proposed.[35–41] The majority of the existing models are based on the assumption of reversible adsorption equilibrium. While this assumption is at odds with the irreversible nature of the adsorption process discussed in Section 2.1, such models may still provide useful insights.

An important class of analytical models is based on density functional theories. These theories normally assume that the adsorbed film is laterally homogeneous, and they attempt to estimate self-consistently the profiles of the concentrations and of the electric potential in the normal direction. Such a self-consistent field (SCF) approach was implemented within a numerical scheme by Fleer and co-workers.[29,35,137] Based on a similar formulation, simple scaling laws could be derived.[138] These approaches are capable of reproducing the frequently

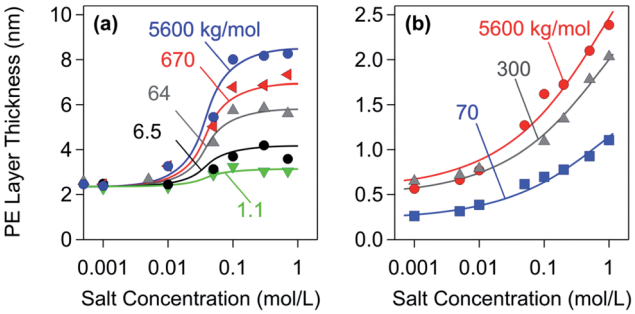

Fig. 5 Layer thickness of saturated PSS layers *versus* salt concentration adsorbed on oppositely charged substrates for different molecular masses of the sodium salt. (a) Amidine latex particles probed with DLS.[32] (b) Planar amino-functionalized silica probed with reflectivity and quartz crystal microbalance.[28]

observed increase of the adsorbed amount with increasing salt concentration, increasing charge density of the substrate, and decreasing charge of the PEs. The SCF approach was also able to provide information concerning the distribution of loops, tails, and trains, to rationalize experimentally observed adsorbed amounts, and to reproduce the maxima in the adsorbed amount for weakly charged PEs.[137,139] Since the adsorbed PE layers are laterally heterogeneous, results obtained from SCF models that assume laterally homogeneous layers must be interpreted with caution. These models are probably most useful to describe the adsorption of weakly charged PEs, which probably form more homogeneous layers.

Computer simulations have also been used to investigate the adsorption of PEs.[39–41] The conformation of a single adsorbed PE chain was studied by considering screened Coulombic interactions only.[39] These authors have found that the adsorbed chain is strongly flattened at low salt concentrations, while it swells at higher salt levels. The simulated normal extensions of the adsorbed PE chain show very similar trends to the measured layer thickness shown in Fig. 5b. This finding strongly supports the view that the layer thickness is determined by the dimensions of individual adsorbed PE chains that are well separated at the surface, leading to a laterally heterogeneous layer. When interactions are governed by electrostatic forces only, this study also confirms that PEs do not adsorb at oppositely charged surfaces above a critical salt concentration.[39,127]

Adsorption of PEs to spherical particles in the presence of salt was recently studied with computer simulations and density functional theories.[40] This approach explains the experimentally observed large accumulation of opposite charge to the particle surface. However, these simulations also predict a maximum in the adsorbed amount at very low salt concentrations, which is at odds with the experiment. All Coulombic interactions were explicitly taken into account in another recent computer simulation study of PE adsorption, whereby effects of short-range hydrophobic attractions were also investigated.[41] This study confirms the view that adsorbed PEs are strongly flattened and that the adsorbed layer is laterally heterogeneous. Unfortunately, the latter study was carried out in the absence of salt, and these conditions are difficult to realize experimentally.

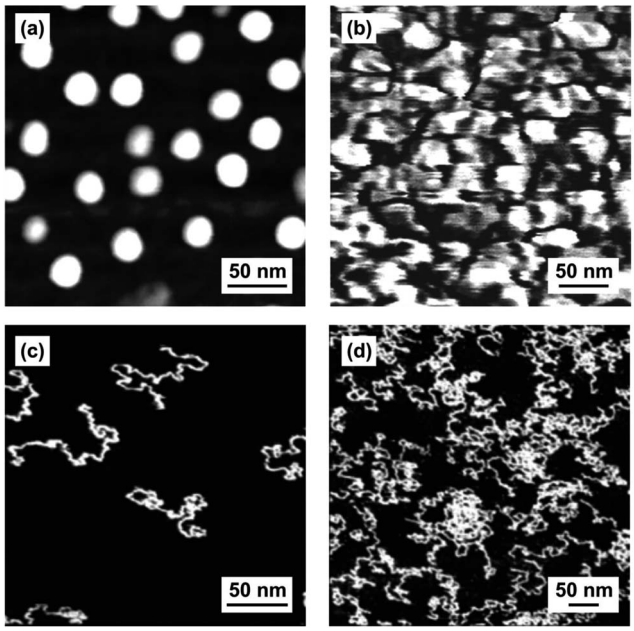

Fig. 6 AFM images of various PEs adsorbed on oppositely charged substrates recorded in air. Saturated layers formed with (a) dendritic PAMAM on mica in pH 4.0 solution without added salt and (b) PSS on amidine latex particles in 1 mM electrolyte solution.[47] Reprinted with permission from *J. Phys. Chem. B*, **113**, 8458. Copyright (2009) American Chemical Society. Unsaturated layers of PVP on mica with (c) small (d) and larger adsorbed amounts.[132] Reprinted with permission from *J. Phys. Chem. B*, **111**, 8597. Copyright (2007) American Chemical Society.

2.3 Charge balance in adsorbed polyelectrolyte layers

Let us now discuss the charge reversal phenomenon and the charge distribution within the adsorbed PE film.

Charge reversal. A most characteristic phenomenon in the adsorption of PEs to oppositely charged substrates is the charge reversal, which is also referred to as overcharging. An adsorbed saturated PE layer has practically always the opposite charge of that of the substrate.[30,31,33,48,93,118,140–147] Exceptions to this rule occur, but only for very weakly charged PEs.[143,144,148] The charge reversal may seem counterintuitive. One might suspect that the PE should be repelled from the substrate, when it attains the same charge as the PE. Since adsorbed PE layers are laterally heterogeneous, only the properties of the surface in the neighbourhood of the adsorption event are important. Therefore, provided an empty spot for adsorption exists, a PE molecule will adsorb. The saturation point of the adsorption is determined through the local environment of the adsorbing chain rather than the overall charge of the surface. Moreover, additional attractive interactions between the PE and the surface exist, for example, hydrophobic or van der Waals forces, and these forces are not influenced by the charge of the substrate.

The overall charge of adsorbed PE layers can be best addressed by electrokinetic techniques. Electrophoresis is the method of choice for colloidal particles, whereby the electrophoretic mobility can be converted into the surface potential (ζ-potential) with appropriate models.[30,48,140–142,148] For planar substrates, streaming potential or streaming current techniques are being used.[33,93] In many situations, this surface potential approximates the diffuse layer potential ψ_D well. When the surface potential is known, the surface charge density σ can be estimated with the Gouy–Chapman relationship[54]

$$\sigma = \frac{2k_B T \varepsilon_0 \varepsilon \kappa}{q} \sinh\left(\frac{q\psi_D}{2k_B T}\right) \quad (13)$$

where the symbols are defined in Section 2.2. Direct force measurements, which will be discussed in Section 3, can be also used to measure surface potentials of colloidal particles and substrates. However, the disadvantage of the latter technique is that in the normally used symmetric situation one can only determine the absolute value of the potential. The sign of the potential must be inferred independently.

The charge reversal upon PE adsorption is illustrated in Fig. 7a and b, where the surface potentials of bare amidine latex particles are compared to those with a saturated adsorbed PSS layer.[131] The data are consistent with the Gouy–Chapman eqn (13) with constant surface charge densities of +5.9 mC m^{-2} for bare particles and −2.6 mC m^{-2} for the coated ones. Besides the different signs, however, the particle coated with the PE behaves very similarly to a bare particle. This observation is not surprising given the fact that the adsorbed PE layer is very thin. The adsorbed PEs are indeed capable of reversing the positive charge of the bare particle and even accumulating substantial additional negative charge at the surface. A good agreement between surface potentials estimated from electrophoresis and direct force measurements is frequently found.[48,107,131,147] In some cases, however, these results disagree, probably due to surface charge heterogeneities.[48]

Fig. 8a illustrates the build-up of this negative charge upon addition of PSS in a suspension of positively charged latex particles.[131] At low PE doses, the particles are positively charged. At a particular dose, the surface charge is neutralized by the PE, and no diffuse layer forms. Upon further PE addition, the negative charge continues to accumulate, until one reaches the saturation point. Before that point is reached, the surface is unsaturated and no PE is dissolved in solution. For doses beyond the saturation point, the adsorbed amount remains constant and the excess PE dissolves in solution.

For unsaturated layers, no free PE is dissolved in solution. This fact can be confirmed in colloidal particle suspensions with electrophoresis experiments at different particle concentrations. Results of such experiments are illustrated in Fig. 8c with carboxylated latex particles and LPEI.[149,150] These particles are negatively charged and adsorbing LPEI leads to a pronounced charge reversal. The collapse of the plots of the electrophoretic mobility *versus* the PE dose for different particle concentrations confirms that the adsorption is quantitative. If this were not the case, there would be a shift of the corresponding curves due to partitioning between adsorbed and dissolved PEs.[151] Adsorbed PSS and PVA on oppositely charged latex particles were shown to behave analogously.[31,140]

The charge reversal of planar charged surfaces induced by adsorption of PEs can be also followed by streaming potential measurements.[33,93,152] These results are illustrated with the adsorption of poly(allyl amine) to mica in Fig. 8d.[152] Bare mica is

negatively charged. At high PE doses, the surface reverses its sign, and the saturation plateau is reached. To avoid the saturation of the surface, the PE solution was in contact with the surface for only 20 min. At lower polymer doses, the surface is unsaturated and passes through the charge reversal.

Charge distribution within the adsorbed film. The normal profiles of the charge density and of the electric potential are depicted in Fig. 7c and d. For a positively charged interface, they are shown in Fig. 7c and they are characterized by a localized layer of charged surface groups. This positive charge is compensated by an accumulation of anions and a depletion of cations in the diffuse layer. For a saturated adsorbed layer of an oppositely charged anionic PE shown in Fig. 7d, the positive charge of the surface is now overcompensated, resulting in a negatively charged surface. This negative charge is neutralized by a diffuse layer where cations are accumulated and anions are depleted.

The charge reversal phenomenon can be captured with a very simple model. One has to assume that the surface charge density of the substrate originates from two additive contributions[107,153]

$$\sigma = \sigma_0 + qZ_{\text{eff}}\Gamma \tag{14}$$

where σ_0 is the surface charge density of the bare substrate and Z_{eff} is the effective charge of the adsorbed PE. The model predictions of the surface potential shown in Fig. 8b reflect the observed trends rather well. The validity of this linear superposition relationship was confirmed in some systems, but disagreement has been reported in others.[30,33,93,152,153]

Adamczyk and coworkers have proposed that this transition is more gradual, which would reflect a decrease of the effective charge with the surface coverage.[33] On the other hand, a sharper transition was observed for latex particles with adsorbed PSS and dendritic PAMAM.[131,153] In the two latter systems, Z_{eff} appears to be constant at first, then increases in magnitude near the charge neutralization point, and again remains constant after this point. Unfortunately, we currently lack a general picture concerning eventual variations of the effective charge of PEs upon changes in the adsorbed amount.

Let us now discuss to what extent the simplified picture shown in Fig. 7d actually reflects the actual charge distribution between the different adsorbed components.[31,109,154] At the charge reversal point, the interface is neutral, and thus the substrate, PE, and the adsorbed salt ions neutralize each other precisely. In some cases, the PE neutralizes the surface exactly, and one refers to stoichiometric adsorption. For other PEs, especially for highly branched ones or for weakly charged surfaces, the counterions of the PEs contribute substantially to the charge balance, and the adsorption is super-stoichiometric. In the case of adsorbed BPEI and PAMAM,[31,155] the counterions may be responsible for the neutralization of up to 90% of the charge originating from the adsorbed PE. In saturated layers, the situation is similar, since the overall surface charge that is neutralized by the diffuse layer is normally just a small fraction of the total charge carried by the adsorbed PE. Furthermore, the lateral heterogeneity will lead to lateral undulations of the

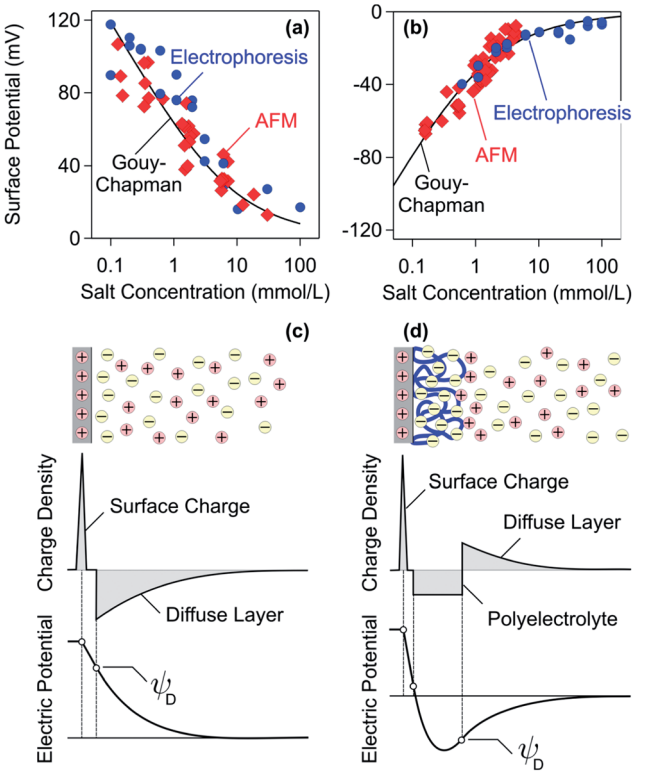

Fig. 7 Comparison of surface potentials for amidine latex particles determined by electrophoresis and direct force measurements by AFM. The solid line is the best fit with the Gouy–Chapman equation. (a) Bare particles and (b) coated with a saturated layer of PSS.[131] Schematic representation of the charge density and the electric potential profiles where the diffuse layer potential ψ_D is indicated. (c) Bare charged interface and (d) charged interface with an adsorbed PE of opposite charge.

diffuse layer. These effects might be responsible for the observed variations of the effective charge with the adsorbed amount of the PE.[153]

A fixed charge stoichiometry of the adsorption process can often be used to rationalize shifts of the charge reversal point. This principle explains why a higher dose of a more weakly charged PE is needed to neutralize the charge of a given surface.[31,50] This trend is also reflected in Fig. 8b. Similarly, a lesser amount of a given PE is needed to neutralize a surface of a smaller surface charge.[150] Dependencies on the solution pH involving weak PEs can be understood similarly. The charge of a weak cationic PE increases with decreasing pH. For a surface with a fixed charge density, the charge reversal point thus shifts towards a higher pH with an increasing amount of adsorbed PE.[143] The same trend is observed for a negatively charged surface with weak acid or amphoteric groups (*e.g.*, silica) in the presence of strong cationic PEs.[110,120] Reverse trends are observed for weak anionic PEs adsorbed on a cationic surface of fixed charge density or for strong anionic PEs adsorbed on a positively charged surface with weak bases or amphoteric groups.[144,148] More complex phenomena are observed when the charges of the PE and of the surfaces are both pH dependent.[4,120,156]

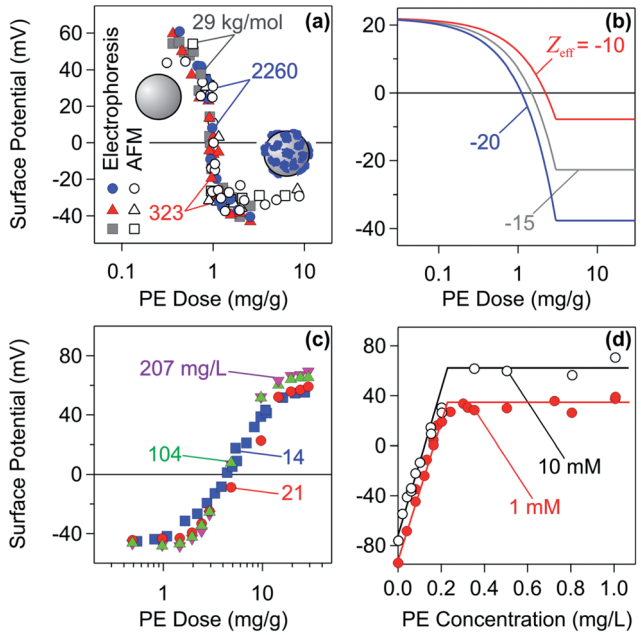

Fig. 8 Charge reversal by adsorbed PEs to oppositely charged substrates in the unsaturated regime as illustrated by surface potential measurements. (a) Amidine latex particles in the presence of PSS of different molecular masses of the sodium salt by electrophoresis and direct force measurements.[47] (b) Calculation of the charge reversal with linear superposition relationship. (c) Electrophoresis measurements of carboxylated latex particles in the presence of LPEI at different particle concentrations.[149,150] (d) Streaming potential measurements of mica in contact with poly(allyl amine) solutions at different electrolyte concentrations indicated for 20 min.[152] Reprinted from *J. Colloid Interface Sci.*, 303, Z. Adamczyk, A. Zembala and A. Michna, PE adsorption layers studied by streaming potential and particle deposition, 353, Copyright (2006), with permission from Elsevier.

The shift of the charge neutralization point for dendritic PAMAM with the molecular mass can be rationalized in a similar way.[155] Due to the compact architecture of these PEs, an increasing number of charged groups will be neutralized by their counterions the higher their molecular mass. Therefore, the effective charge increases more slowly than the molecular mass, thus the charge neutralization point shifts toward higher PE doses. However, this effect is absent for linear PEs. They adsorb in a much flatter configuration, and therefore the charge stoichiometry is independent of the molecular mass.

3 Forces induced by polyelectrolytes

In this section, we will discuss measured force profiles between charged surfaces or between particles with adsorbed polyelectrolytes (PEs) of opposite charge. An important observation will be that the classical DLVO theory describes forces in such systems reasonably well. Additional attractive non-DLVO forces have been identified and can be important under certain conditions, especially for PEs of high charge density and high molecular mass. These additional forces are largely of electrostatic origin and result from the laterally heterogeneous patch–charge distribution within the adsorbed PE film. Additional attractive forces may occur due to bridging of PE chains or due to depletion at higher PE concentrations.

DVLA forces. The force F acting between two charged objects across an aqueous electrolyte solution is assumed to have two main contributions[54,157]

$$F = F_{vdW} + F_{dl} \quad (15)$$

namely, the attractive van der Waals force F_{vdW} and the repulsive electric double layer force F_{dl}. The van der Waals force originates from dispersive interactions between permanent and fluctuating dipoles of the constituent molecules. For a pair of particles of radius R this force can be approximated as

$$F_{vdW} = -\frac{RH}{12h^2} \quad (16)$$

whereby the Hamaker constant H characterizes its strength. This expression is valid when the surface separation h is small with respect to the particle radius R. This assumption is applicable when retardation effects are negligible and when the Derjaguin approximation is invoked. The double layer force can be viewed to originate from the osmotic pressure resulting from the overlap of the diffuse part of the double layers. Within the Derjaguin approximation, the force acting between two identical particles can be expressed at larger distances as

$$F_{dl} = 2\pi R\varepsilon_0\varepsilon\kappa\psi_{eff}^2 e^{-\kappa h} \quad (17)$$

where ψ_{eff} is the effective electric potential. For a weakly charged surface, this quantity is equal to the surface potential. For a highly charged surface, the Poisson–Boltzmann theory suggests that it converges to a constant value given by $\psi_{eff} = 4k_BT/q$.[158] This relationship is analogous to the previously mentioned relationship between the effective charge Z_{eff} and bare charge Z. The expression for the double layer force invokes the superposition approximation, which stipulates that the diffuse layer does not deform upon approach. At shorter distances, charge regulation or non-linearities may become important, but in many cases eqn (17) remains a good approximation. More accurate treatment on the mean-field Poisson–Boltzmann level normally relies on numerical solutions of the corresponding differential equation.

3.1 Bare surfaces and surfaces with saturated PE layers

As discussed in Section 2.1, saturated layers form when the adsorbing PE is added in sufficiently large quantities. Such layers are normally thin and highly charged. Therefore, forces between these layers mainly originate from double layer interactions. In the following, we will discuss forces between bare surfaces first, and then between surfaces coated with saturated PE layers.

Bare surfaces. Fig. 9a shows typical force profiles between negatively charged sulfate latex particles measured with the colloidal probe technique at low salt concentrations.[48] The double layer interaction follows an exponential force law. The

range of this force corresponds to the thickness of the diffuse layer, which is given by the Debye length, κ^{-1}. This length decreases with increasing salt levels, as predicted by eqn (11). The intercept reflects the strength of the interaction and is related to the surface potential. The experimentally measured forces are perfectly consistent with DLVO theory, which is represented by the solid lines in Fig. 9. Similar double layer forces have been observed between other types of charged particles, such as positively charged latex, silica, or other materials.[131,159,160] Electrostatic potentials determined from the force profiles typically agree well with ζ-potentials obtained from electrophoresis, especially for weakly charged surfaces, while for highly charged particles the magnitude of the observed ζ-potentials tends to be higher.[48,131,161]

The forces become attractive at shorter distances, but this attraction cannot be well resolved due to the inherent mechanical jump-in instability.[162] During this instability, deviations from DLVO theory are mainly caused by hydrodynamic drag. This drag creates additional repulsive forces, which mask the attractive forces at short distances. The force measurements shown were carried out at relatively low salt levels, where double layer forces dominate. Similar force measurements at higher salt levels or for weakly charged particles have been reported more recently, and they reveal the expected attractive van der Waals forces.[163] These results confirm that the DLVO theory also correctly describes the transition between attractive and repulsive forces in such systems.

Similar force measurements between charged solid interfaces across aqueous solutions of monovalent electrolytes have been carried out with the SFA and the colloidal probe in the sphere–plate geometry.[161,164–166] In the latter case, the symmetry of the system remains difficult to ascertain. Nevertheless, these studies confirm that forces in such systems are consistent with the simple DLVO picture, at least down to distances of few nm.

Surfaces coated with saturated PE layers. When a charged substrate is incubated in a sufficiently concentrated solution of oppositely charged PEs, a saturated PE layer will form. This layer is thin and highly charged, and thus forces acting between such coated surfaces will be dominated by electrical double layer interactions. Fig. 9b illustrates this situation by reporting force profiles between sulfate latex particles coated with a saturated layer of cationic LPEI.[48] The forces resemble the ones acting between the corresponding bare charged surfaces shown in Fig. 9a. At low salt levels, these profiles are again strongly repulsive and can be well described by DLVO theory. Thereby, a Hamaker constant of 4.0×10^{-21} J has been used to model interactions between latex particles across aqueous electrolyte solutions and the same value will be used subsequently. The only difference is that the bare surfaces are negatively charged, while the coated ones are positively charged. Since the square of the surface potential enters eqn (17), these forces do not depend on the sign of the surface potential. The fact that interaction forces between bare particles and between PE-coated particles are similar is not surprising given the fact that PEs adsorb in a thin layer. PE-coated surfaces simply behave as any other charged interface. For surfaces coated with PEs, force and electrophoresis measurements typically yield very similar electric surface potentials.[48,131] The congruence between these two techniques is also illustrated in Fig. 8a.

Numerous other studies confirm that interactions between surfaces coated with saturated PE films are governed by repulsive double layer forces. Such a behaviour was observed for positively charged amidine particles coated with the anionic PSS[131] and for negatively charged sulfate latex particles in the presence of cationic LPEI and dendritic PAMAM.[48,107] Double layer forces were observed between silica, mica, or functionalized surfaces in the presence of various oppositely charged PEs.[72,109,167–175] The strength of double layer forces could also be varied through solution pH.[72,147,176] This dependence originates from the resulting variation of the dissociation degree of the PE. In some cases, deviations from DLVO theory have been reported at short distances, and they were either attributed to steric repulsion[168,169,177,178] or to patch–charge attraction.[48,107,131] However, these contributions are rather weak and one can conclude that double layer forces dominate the interactions between charged substrates with saturated PE layers of opposite charge.

Bridging polymer chains are known to induce additional attractive forces, and this mechanism was suggested to be important for PEs as well.[43,179,180] Such bridging processes can be probed directly with the AFM, and this approach is referred to as single molecule force spectroscopy.[109,181–183] The principle is illustrated in Fig. 10. The force profiles are normally measured through a repeated approach and retraction cycles of the probe with respect to the surface, and the surfaces remain in contact for short periods of time. When the surfaces are in proximity, some of the PE chains adsorbed to one of the surfaces may adsorb to the other surface and thereby bridge both surfaces. The existence of such bridging PE chains is easily detected during the retraction of the probe, since these chains are being stretched and detached from the surfaces. These processes lead to characteristic spikes or plateaus in the retraction force curves.

Bridging events were investigated in detail for saturated layers of adsorbed PVA on silica by force measurements with AFM.[109,182] Representative examples are shown in Fig. 10. When the PE chain is anchored strongly to both surfaces, the chain is

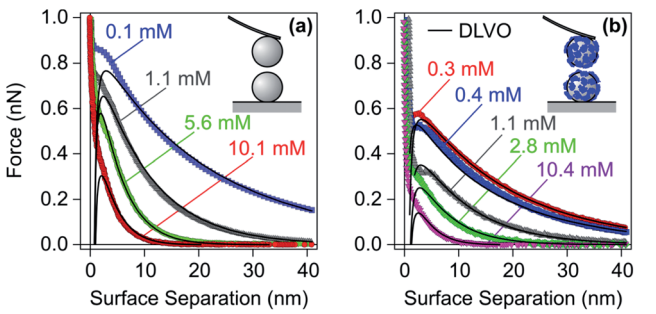

Fig. 9 Experimental force profiles for sulfate latex particles in monovalent electrolyte solutions adjusted to pH 4.0 compared with their best fits by DLVO theory. (a) Bare negatively charged particles and (b) the same particles at a LPEI dose of 1.1 mg g^{-1}, which results in a saturated adsorbed PE layer of positive charge.[48]

stretched, which leads to a characteristic spike. This situation is referred to as pulling and is shown in Fig. 10a. When the anchoring to one of the surfaces is weaker, the chain will detach continuously, which will lead to a plateau in the force curve. Here we refer to peeling, which is shown in Fig. 10b. More complex events equally occur and they are illustrated in Fig. 10c and d. Similar experiments were equally used to obtain information about the loop distribution of the adsorbed PEs.[184]

While such bridging processes are rare at low salt levels, they become rather frequent at higher salt concentrations and for weakly charged PEs.[109] Similar observations could be made for saturated BPEI films.[169] This trend can be rationalized since the adsorbed layers were thin under low salt conditions, and the PE chains are strongly bound to the substrate by attractive electrostatic forces. As the salt level increases, these attractive forces are screened, thus allowing PE chains to explore the regions further away from the surface. In this case, bridging becomes more frequent. Under these conditions, however, the forces are often completely attractive, and the presence of additional attractive bridging forces may not modify the picture substantially.

3.2 Surfaces coated with unsaturated layers

At lower PE doses, one obtains unsaturated layers, which feature lower adsorbed amounts than the saturated ones. As discussed in Section 2.2, adsorbed unsaturated layers are often laterally heterogeneous, but they can also be more homogeneous in some situations. Nevertheless, the principal contributions to the force can be again understood within DLVO theory. Let us first discuss the forces in the simpler case of laterally homogeneous layers, and later address the more complex situation of heterogeneously adsorbed layers.

Homogeneous polyelectrolyte layers. Fig. 11 shows the interaction forces between negatively charged sulfate latex particles at pH 4.0 for different doses of cationic LPEI.[48] Solid lines are best fits with DLVO theory. When no PE is added, the forces are dominated by double layer repulsion. As the PE dose increases, the surface charge is progressively neutralized, and the repulsive forces weaken. The charge reversal point is located near a dose of 0.28 mg g^{-1} (0.15 mg m^{-2}), where one observes attractive van der Waals forces only. As the dose is increased further, a positive charge builds up, and the forces become repulsive again. At doses above 1.0 mg g^{-1} (0.55 mg m^{-2}), the surface becomes saturated and the repulsive forces do no longer increase. The effect of an adsorbing PE results from the modification of the surface charge, and the forces can be well described by DLVO theory across the entire range of the PE dose. As shown in Fig. 11, theoretical DLVO predictions follow the experimental data accurately. Since DLVO theory is applicable, we suspect that the adsorbed LPEI layers are rather homogeneous. These layers are likely to be homogeneous on length scales exceeding the Debye length, which is about 10 nm in this case. In the repulsive force profiles, the short-range attractive part cannot be well resolved due to the jump-in instability. Heterogeneously charged layers would show additional attractive non-DLVO forces.

Force measurements for unsaturated PE layers near the charge neutralization point are difficult to perform, and therefore only few such reports are available.[48,107,131,176,185] The main obstacle is that charge neutralization can be only achieved in a narrow range of PE doses, and this condition is difficult to realize for the small surface areas available in the currently used force measurement protocols. From this point of view, the SFA or its variants are more advantageous, since the surface area is few cm^2. The surface area of a single particle used in the colloidal probe experiment is only few μm^2, whereby the necessary PE doses are minute and they cannot be properly controlled. The recently described multi-particle colloidal probe technique circumvents this problem by depositing a larger number of particles to a substrate.[48,107,131] In this fashion, one may again reach surface areas of several cm^2, for which the necessary dose is simpler to control. Another possibility is to work with low PE concentration and to monitor the force profiles with time.[185] In such an experiment, the system initially passes through the charge neutralization point, while the saturated layer forms later.

Another possibility is to prepare a saturated layer with a weak PE and to neutralize the charge by adjusting the solution pH. With this technique, adsorbed PVP layers were shown to interact by pure van der Waals interactions at their charge neutralization point.[176] This finding suggests that these PVP films are also laterally homogeneous, similar to the ones formed with LPEI.[48] One may hypothesise that partially protonated LPEI and PVP form homogeneous adsorbed layers due to lowering of the PE charge by deprotonation and the presence of additional hydrophobic interactions.

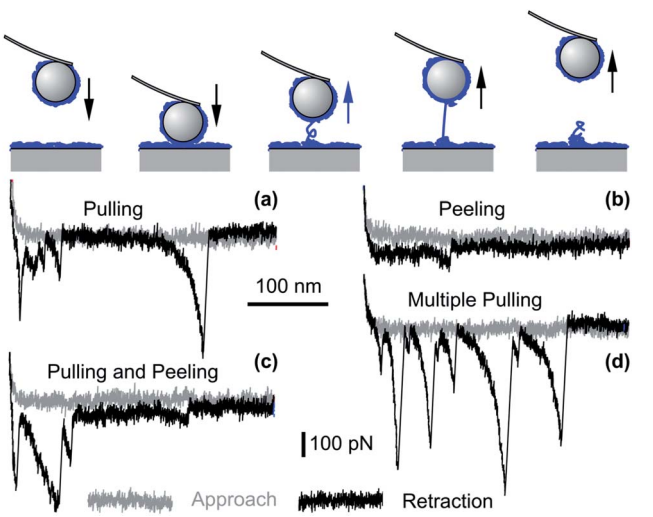

Fig. 10 Bridging events as probed by colloidal probe AFM force measurements for saturated PVA layers of molecular mass of 520 kg mol^{-1} adsorbed to silica in 100 mM electrolyte solution of pH 4.0. Single molecule (a) pulling and (b) peeling events. More complex events involving several molecules may show (c) a combination of pulling and peeling events and (d) multiple pulling events.[109]

Heterogeneous polyelectrolyte layers. Most experiments conducted on adsorbed PE layers indicate that forces involve additional attractive interactions. We suspect that such an attraction principally originates from the lateral heterogeneity of the adsorbed PE layers and the resulting patchy charge distributions. In this case, the interaction force can be approximated as[186,187]

$$F = F_{vdW} + F_{dl} + F_{pc} \quad (18)$$

Besides the two first terms, which correspond to the DLVO contribution, the additional term F_{pc} reflects the attractive non-DLVO force due to patch–charge attraction.

Fig. 12 shows interaction forces between amidine latex particles neutralized with PSS at a dose of 1.0 mg g^{-1} (0.58 mg m^{-2}).[131] One observes that the attractive forces are substantially stronger than the van der Waals force expected from DLVO theory, especially for high molecular mass and at low salt levels. Experimental force profiles can be well fitted when this additional non-DLVO force is assumed to be exponential

$$F_{pc} = -Ae^{-qh} \quad (19)$$

This exponential dependence was also found theoretically by analysing interactions between surfaces with a periodic charge distribution.[186,187] This analysis indeed yields an additional attractive interaction. This attraction results from the preferential orientation of the positively charged patches such that they face the negatively charged ones. Such patch–charge attractive forces are the strongest when the surface charge heterogeneities form a regular lattice, but these forces are also expected to be operational when the patches are arranged in a liquid-like fashion. The theoretical analysis relates the decay length q^{-1} of this interaction to the Debye length by the simple expression[186]

$$q^2 = \kappa^2 + \left(\frac{2\pi}{b}\right)^2 \quad (20)$$

where b is the lattice spacing. At low salt levels, the range of this force is governed by the lattice spacing, while at higher salt levels, the force is screened as a regular double layer force. The data shown in Fig. 12a can be described by $b = 15$ nm. This number agrees roughly with the size of the structures revealed by AFM imaging shown in Fig. 6b. With increasing salt concentrations, the patch–charge attraction is screened and at higher salt levels the forces are again described by DLVO theory. In that case, a Hamaker constant of 9.0×10^{-21} J was used but the plane of origin was shifted to account for effects of roughness. Fig. 12b illustrates that the size of the surface heterogeneities also plays an important role. Their size decreases with decreasing molecular mass, and the additional non-DLVO force disappears.

Very similar results were obtained by direct force measurements between negatively charged sulfate latex particles in the presence of dendritic PAMAM.[107,188] Near the charge neutralization point, forces are attractive, and they are again much stronger than the van der Waals force, especially for high molecular mass and low salt levels. The additional attraction can be again rationalized with the exponential relationship given in eqn (19). The measured corresponding lattice spacing of this particular system is about $b = 16$ nm, but this value is substantially smaller than the nearest neighbour spacing of the dendrimers at the surface, which is about 50 nm. This discrepancy probably originates from the assumption of a square lattice inherent to the patch–charge model, while the actual surface structure is irregular.

Additional attractive forces near the charge neutralization point were reported in other systems with the SFA or related techniques.[185] By exploiting the kinetics of the adsorption process, attractive forces near this point could be observed for PVA films at low salt levels.[185] These forces were equally reported to be exponential and substantially more attractive than the van der Waals forces. We suspect that these forces also originate from patch–charge attraction. Similar non-DLVO attractive forces were reported between layers of adsorbed poly((3-methacrylamido)-propyl)trimethylammonium chloride on mica.[42]

Polymer bridging might also lead to additional attractive forces. As discussed above, bridging events can be detected with the AFM in the retraction part of the force curves, as shown in Fig. 10. The occurrence of such bridging events was analyzed near the charge neutralization point for the LPEI and PSS systems.[47,48] While such events could be observed, they occurred at low salt concentrations very rarely. Moreover, forces observed in the PSS and PAMAM systems are similar, in spite of the fact that the PE architectures are very different. If bridging would be important, one expects substantial differences between the forces in these two systems.

At higher salt levels, where bridging forces are expected to be operational, the DLVO theory also predicts attractive forces. Therefore, additional attractive bridging forces may not alter the scenario much. At intermediate salt levels, however, where the strength of double layer forces and van der Waals forces are comparable, additional bridging forces may influence the picture considerably. Similarly, when the charge of the PEs is low, bridging forces might become important in analogy to neutral polymers.[189] This suggestion is supported by more frequent occurrences of single molecule bridging events

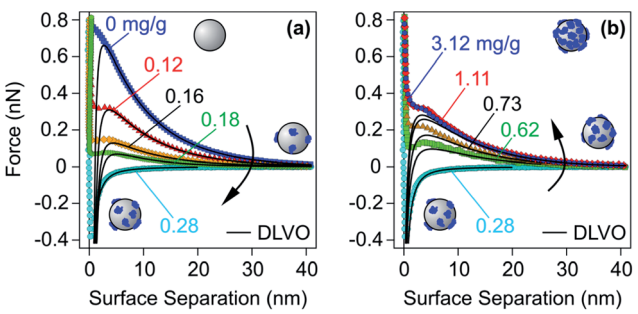

Fig. 11 Experimental force profiles for sulfate latex particles for different doses of LPEI at an ionic strength of 1.1 mM adjusted with a monovalent salt at pH 4.0 compared with their best fits by DLVO theory.[48] PE doses (a) below and at the charge reversal point and (b) at the charge reversal point and above.

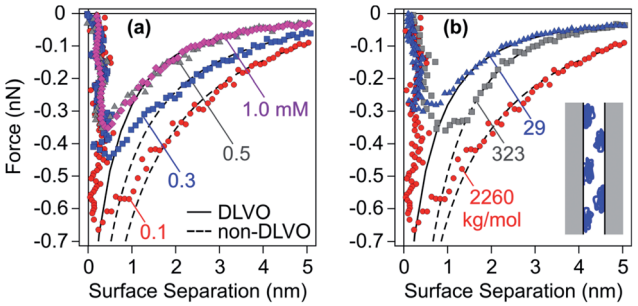

Fig. 12 Attractive force profiles for amidine latex particles neutralized with adsorbed PSS in monovalent salt solutions at pH 4.0 together with best fits by DLVO theory (solid lines) and additional patch–charge attraction (dashed lines).[47] The force curves might be inaccurate close to contact due to eventual jump-in instability. (a) Molecular mass of 2260 kg mol^{-1} at different ionic strengths and (b) different molecular masses at an ionic strength of 0.1 mM. The scheme illustrates the patch–charge attraction mechanism.

observed with the AFM under these conditions.[178,190] However, the precise conditions where bridging forces become important remain unclear to us.

Interactions between surfaces in the presence of PEs were investigated theoretically in detail by density functional theories and computer simulations.[191,192] Density functional theories suggest that interactions can be indeed described by DLVO theory at larger distances. Computer simulations were used to model forces between surfaces by approximating the PEs as charged spheres that interact by means of screened Coulombic interactions. These simulations confirmed the importance of DLVO forces, but also suggested additional short-range interactions originating from ordered arrangements of the PEs at the surface.[188] A similar study with flexible PE chains, which included all Coulombic interactions explicitly, found similar additional attractive forces, but the range of the forces did strongly depend on the chain flexibility.[193] Attractive forces close to charge neutralization and repulsive forces away from this point were also reported.[194] These studies demonstrate the importance of additional attractive forces. Other computer simulation studies suggest that bridging forces might also be important.[195–198] However, these studies refer to bridging even when PEs are not absorbed at both surfaces and these simulations are carried out under equilibrium conditions. The irreversible nature of the adsorption process and the resulting slow dynamics of the adsorbed chains may modify the nature of the bridging contributions substantially. On the other hand, the adsorbed PE chains may maintain some lateral mobility and equilibrate laterally to some extent.

Depletion forces. At higher PE concentrations, typically above few g L^{-1}, and for non-adsorbing or weakly charged polymers, depletion forces become important.[44,45,196,199–204] Such forces result from the mismatch in the osmotic pressure within the gap between two approaching particles and the bulk solution. When the gap is small compared to the size of the PE coil, the PE concentration in the gap is smaller, leading to an attractive force between the particles. At higher PE concentration, these forces may become oscillatory, as they reflect the structuring of the PE bulk solution. Depletion forces are well documented in PE solutions involving non-adsorbing surfaces.[44,200–202] As expected, depletion forces increase in strength with decreasing salt levels and increasing molecular mass of the PE. Depletion forces acting between surfaces saturated with oppositely charged PEs were reported as well.[45,203] These forces were suggested to set in already at moderate PE concentrations, and no oscillatory forces were observed in this case. The latter effect might be related to the presence of lateral surface heterogeneities of the adsorbed PE layers and may reflect similar modifications of depletion forces as induced by substrate roughness in particle suspensions.[205]

4 Particle aggregation induced by polyelectrolytes

Aggregation of colloidal particles is governed by the interaction forces acting between the particles. Simplistically, attractive forces lead to rapid particle aggregation, while this process is slowed down by repulsive forces. The elementary step of the aggregation process can be viewed as a chemical reaction

$$A + A \rightarrow A_2 \tag{21}$$

whereby a particle dimer is being formed from two monomeric particles. The formation rate of the dimers is given by[54,206,207]

$$\frac{dN_2}{dt} = \frac{k}{2} N_1^2 \tag{22}$$

where N_1 and N_2 are the number concentrations of the monomers and dimers, respectively, and k is the aggregation rate coefficient. The aggregation process does not stop with the formation of dimers, but continues through higher order aggregates.[54,206,207] These aggregates have an irregular, ramified structure and can be characterized as mass fractals. These aggregates may interlink such that finally only one large aggregate spans the entire container. In that case, one refers to the formation of a colloidal gel.[208–210]

Aggregation rates from DVLO theory. The key contribution of DLVO theory was to derive the aggregation rate coefficient in terms of the interaction potential between colloidal particles. From the steady-state solution of the forced diffusion equation one finds that the rate coefficient is given by[52–54,206]

$$k = \frac{4k_B T}{3\eta R}\left[\int_0^\infty \frac{\beta(h/R)}{(2R+h)^2}\exp[V(h)/(k_B T)]dh\right]^{-1} \tag{23}$$

where η is the viscosity of the solution, $V(h)$ is the interaction potential energy, and $\beta(x)$ is the hydrodynamic resistance function at $x = h/R$. The interaction potential can be obtained by integrating the force profile

$$V(h) = \int_h^\infty F(h')dh' \tag{24}$$

while the resistance function can be approximated as[206,211]

$$\beta(x) = \frac{6x^2 + 13x + 2}{6x^2 + 4x} \tag{25}$$

DLVO theory predicts two regimes for the aggregation processes.[54,206] The first regime, referred to as the fast or diffusion controlled aggregation, typically occurs for high salt concentrations or small surface charge densities. In this situation, the aggregation rate coefficient is approximately given by the Smoluchowski value for hard spheres[54,206]

$$k = \frac{8k_B T}{3\eta} \simeq 1.2 \times 10^{-17}\ \mathrm{m^3\ s^{-1}} \tag{26}$$

where the numerical value refers to water at room temperature. This expression can be obtained from eqn (23) by setting the exponential factor and the resistance function to unity. Experimentally observed aggregation rates in the fast regime are normally comparable to the Smoluchowski value, but they are often somewhat smaller.[211–215]

The second regime, referred to as the slow or reaction controlled aggregation, occurs at lower salt concentrations and higher surface charge densities. In this case, the interaction potential develops a barrier, which leads to a small aggregation rate coefficient. The relatively sharp transition between these two regimes is referred to as the critical coagulation concentration (CCC). This transition has been observed in numerous systems, for example, as a function of the salt concentration,[215,216] or when the surface charge density was varied by adjusting the solution pH.[212–214] The DLVO theory is capable of describing the aggregation rates accurately provided that the surface charge density is not too high.[212] At higher surface charge densities, important deviations may occur.

The aggregation rate coefficients are normally reported as the stability ratio defined as[54,212]

$$W = \frac{k_{\mathrm{fast}}}{k} \tag{27}$$

where k_{fast} is the aggregation rate coefficient in the fast regime of a reference system, typically at high electrolyte concentrations, and k is the rate coefficient under the conditions in question. Therefore, the stability ratio is close to unity in the fast aggregation regime, and it increases as the aggregation slows down.

4.1 Bare particles and particles with saturated PE layers

Aggregation rate coefficients of colloidal particles can be accurately measured with time-resolved light scattering, turbidity, or single particle counting.[207,217,218] In many situations, the trends observed can be well rationalized by DLVO theory. In the following, we will discuss aggregation rates in suspensions of bare particles first and then in suspensions with particles coated with saturated PE layers.

Bare particles. Aggregation rate coefficients of bare colloidal particles were reported in numerous studies.[207,212–214,216,219–222] The characteristic dependence of the stability ratio for charged sulfate and amidine latex particles on the concentration of monovalent salt is shown in Fig. 13a. The solid line represents the stability ratio calculated with DLVO theory whereby the electrical surface potentials were estimated by electrophoresis. Experimental and calculated stability ratios show the regimes of slow and fast aggregation, and they feature a similar dependence on the salt concentration. In the fast aggregation regime that is encountered at high salt concentrations, the stability ratio is close to unity and constant. In the slow aggregation regime, the stability ratio increases rapidly with decreasing electrolyte concentration. The CCC is located at the transition between these two regimes and lies near 0.2–0.3 M, which is typical for highly charged particles in a monovalent salt solution.

A common difficulty with DLVO theory is that it predicts a substantially stronger dependence of the stability ratio on the salt concentration than that observed experimentally. In this example, this discrepancy is apparent in the slow aggregation regime by the different slopes of experimental data and of the DLVO calculations. A similar behaviour and analogous discrepancies with theoretical predictions have been reported in other systems containing charged particles in the presence of monovalent salts.[216,219–223] The origin of this discrepancy is probably related to lateral patch–charge heterogeneities.[214,220,223–225] These patch–charge heterogeneities that are also likely present on the bare particles have a different origin than the ones discussed above, which originate from the lateral heterogeneity of the adsorbed PE films. The patch–charge heterogeneities of the bare particles may originate from the discreteness of the charged groups or an uneven distribution of these groups at the surface that result from the synthesis process. Their presence was also evidenced by differential electrophoresis techniques.[226] These heterogeneities will equally induce additional attractive forces. Such attractions are expected to be stronger between particles suspended in solution than those measured with the colloidal probe AFM. Suspended particles can rotate freely and they will eventually find a configuration of the patches on the two particles involved that lead to an approach pathway of the lowest free energy.

In the fast regime, DLVO theory predicts an absolute rate constant of $7.1 \times 10^{-18}\ \mathrm{m^3\ s^{-1}}$. The fact that this value is smaller than Smoluchowski's value given in eqn (26) originates from the interplay between van der Waals forces and hydrodynamic interactions. The experimentally measured aggregation rate coefficient is $3.5 \times 10^{-18}\ \mathrm{m^3\ s^{-1}}$ for the sulfate latex particles and $4.4 \times 10^{-18}\ \mathrm{m^3\ s^{-1}}$ for the amidine latex. These values are smaller than the ones predicted by DLVO theory, and the remaining discrepancies probably originate from inaccuracies of the hydrodynamic resistance function at small separations.

Particles coated with saturated polyelectrolyte layers. Trends concerning the stability of particles coated with a saturated polyelectrolyte (PE) film are very similar to bare particles, suggesting that the principal interactions are governed by DLVO forces too.[141,142] Fig. 13b shows data of negatively charged sulfate latex particles coated with cationic PDDA and of positively charged amidine latex particles coated with anionic PSS. They are compared with DLVO calculations whereby surface potentials were estimated from electrophoresis. The characteristic regimes of slow and fast aggregation can be identified as well. Again, the DLVO theory predicts a stronger dependence of

the stability ratio on the salt concentration in the slow regime. This dependence seems even weaker than for the bare particles, suggesting that the patch–charge heterogeneities are more pronounced for the saturated PE layers than for the bare particles. For the particles coated with PEs, the CCC is shifted to higher salt concentrations and the stability ratio exceeds unity in the fast regime. This small increase in the stability ratio is probably due to additional contributions from repulsive steric forces originating from overlapping PE layers. Such additional forces may also lead to higher CCCs, but the more likely origin of this shift is the high surface charge density of saturated PE layers.

The similarity between bare colloidal particles and particles coated with a saturated PE layer was observed for various other systems, including negatively charged sulfate latex particles in the presence of LPEI, positively charged amidine latex particles in the presence of PSS or PAA, and hematite particles with alginate.[142,227] A similar behaviour was also reported for latex particles with poly(methacrylic acid) grafted to their surface.[228] This similarity is further supported by direct force measurements, which indicates that interactions between surfaces coated with saturated PE layers are well described by DLVO theory as illustrated in Fig. 9b. These findings clearly demonstrate that forces acting between the charged surfaces and those coated with a saturated PE layer are similar and that they can be understood within DLVO theory. This similarity is due to the very thin and compact nature of the adsorbed PE films.

Particles with an adsorbed saturated PE layer often have higher CCCs.[141,142] Particles with grafted PEs on their surface have CCCs in monovalent salts even above 1 M.[228,229] Saturated adsorbed PE films typically feature high surface charge densities, which will cause the CCC to shift to high salt concentrations. However, the systems shown in Fig. 13b are characterized by stability ratios larger than unity in the fast aggregation regime, pointing to a more stable suspension than the one predicted theoretically, even at high ionic strengths. Stabilization at high salt levels was also observed in the presence of neutral polymers or for grafted PE brushes.[221,228,229] This effect is sometimes referred to as electrosteric stabilization.[199,221,228] This additional stabilization cannot be rationalized within DLVO theory, but reflects additional repulsive steric forces. However, such effects are not very important in charged particle suspensions in the presence of oppositely charged PEs.[141,142,230]

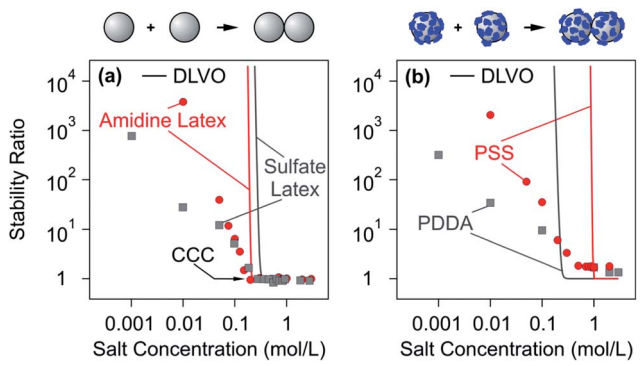

Fig. 13 Dependence of experimentally measured stability ratios of latex particles on monovalent salt concentration at pH 4.0 and comparison with DLVO theory. (a) Bare amidine latex and sulfate latex particles and (b) the same particles coated with a saturated layer of PSS and PDDA, respectively.[140,142] Schemes on the top illustrate the dimer formation without and in the presence of PEs.

4.2 Aggregation involving unsaturated polyelectrolyte layers

Stability ratios pass through a characteristic minimum with increasing PE doses. Since unsaturated PE layers undergo a charge reversal with increasing the mass of adsorbed PE, this dependence can be rationalized by DLVO theory. Adsorbed unsaturated layers are often laterally heterogeneous, but sometimes they can be more homogeneous. Let us now discuss the aggregation rates of particles in suspension in such situations. We will first focus on the simpler case of homogeneous layers and discuss heterogeneous layers later.

Homogeneous polyelectrolyte layers. The characteristic dependence of the stability ratio on the PE dose and the influence of the added monovalent salt are illustrated in Fig. 14. The example shown refers to negatively charged sulfate latex particles in the presence of LPEI in an electrolyte solution at pH 4.0.[150] Under these conditions, the ionization degree of LPEI is about 65%.[231] At low salt concentrations, one observes the characteristic U-shaped stability plot. The suspension is stable at low PE doses. With increasing doses, the stability ratio decreases, until it reaches unity near the charge neutralization point. This point is located near 0.8 mg g^{-1} (0.04 mg m^{-2}). When the PE dose is increased further, the suspension is stabilized again. At higher salt concentrations, one observes plateaus in the stability ratio at both low and high PE doses. These plateau values diminish rapidly with increasing salt concentrations, and for high salt concentrations the fast aggregation regime is reached for any PE dose. The salt dependence of these plateaus is better reflected in the stability plots *versus* the salt concentration for the bare and PE-coated particles, while the onset of fast aggregation is defined by the corresponding CCCs. This situation was discussed above and is illustrated in Fig. 13.

Let us compare these results with predictions of DLVO theory, whereby the surface potentials were estimated from electrophoresis. At low salt concentrations, DLVO theory reproduces the experimental data well. The likely reason why DLVO theory works in this case is that the adsorbed LPEI film is laterally homogeneous. Force measurements shown in Fig. 11 also suggest that the film is homogeneous on length scales of at least 10 nm. This number is in agreement with the present stability data, since DLVO predictions break down for salt concentrations near and above 10 mM. While the minimum is described reasonably well, the plateau at high LPEI doses is no longer located properly. While the DLVO theory is capable of predicting the overall shape of the stability curve at higher salt concentrations qualitatively, it fails to do so quantitatively. The predicted widths of the instability region and the values of the stability plateaus do not agree with experiments. At higher salt levels, the system is more stable than what is predicted by DLVO theory, possibly due to steric forces.

Another experimental finding confirming the homogeneity of adsorbed LPEI layers is presented in Fig. 15a. This graph shows experimental stability data for different molecular masses.[150] No significant trend with the molecular mass can be established and a good agreement with DLVO theory is observed.

There are numerous other reports confirming that the aggregation near the charge reversal is rapid and that it slows down away from this point. They involve a wide range of PEs together with positively[49,140,144,148,232] and negatively charged particles.[31,49,50,56,110,142,145,155] However, the plateaus in the stability ratios at high and low PE dose are difficult to observe experimentally, and therefore they are often missing. Nevertheless, the existence of these plateaus has been clearly demonstrated in some systems.[141,142,148,150]

With increasing salt concentration, the fast aggregation regime widens and the dependence of the rate coefficient on the PE dose weakens in the slow regime. This salt dependence is generic and was reported for negatively charged latex and silica particles in the presence of cationic PEs[31,49,110,142,155] and for positively charged latex particles with PSS or PAA.[140,148]

Heterogeneous polyelectrolyte layers. Adsorbed PE films are often laterally heterogeneous, and in this situation the aggregation is faster due to the attractive patch–charge interactions.

Fig. 15b shows aggregation rates of sulfate latex particles in the presence of dendritic PAMAM of different molecular masses.[155] When the molecular mass is small, the dependence of the stability ratio on the PE dose is relatively well described by DLVO theory. For large molecular masses, however, the experimentally observed stability ratios are substantially smaller than the predicted ones. Attractive patch–charge interactions between heterogeneous surfaces are likely to be responsible for this reduction. When one approximates these interactions with eqn (19), the experimentally observed trend can be captured relatively well. The higher the molecular mass, the larger the size of the patches, and this increase leads to a larger range of attractive non-DLVO forces; see eqn (20). The stability measurements were carried out at a salt concentration of 1 mM, which corresponds to a Debye length of 10 nm. The nearest-neighbour distances between the dendrimers are below this value for the molecular mass of 3.3 kg mol^{-1}, and thus the film should be considered homogeneous. The shift of the minimum in the stability plot shown in Fig. 15b reflects the shift in the charge neutralization point. This effect is discussed in Section 2.3 and is related to the compact architecture of dendritic PAMAM.

The role of patch–charge heterogeneities is typically manifested in the stability plots by widening of the fast regime and weaker dependence in the slow regime. These trends could also be well predicted by Monte Carlo simulations, where the dendritic PAMAM were modelled as charged hard spheres interacting with screened Coulomb potential.[233]

Similar dependencies on the molecular mass were observed for amidine latex particles in the presence of PSS or PAA,[140,148] for cationic PEs and sulfate latex,[56] or silica particles.[234,235] However, no dependence of the stability ratio on the molecular mass is observed for LPEI, as illustrated in Fig. 15a.[150] This

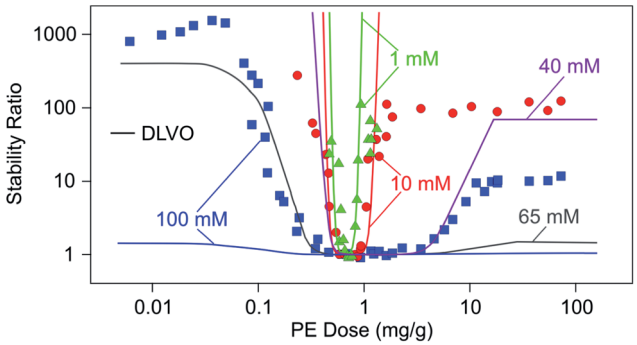

Fig. 14 Stability ratios of sulfate latex particles *versus* the dose of LPEI at different ionic strengths adjusted by a monovalent electrolyte and at pH 4. Solid lines are calculations with DLVO theory.[150] Note that only calculated curves are shown for 40 mM and 65 mM. These calculations illustrate that DLVO theory reproduces the overall dependence correctly, albeit not at the appropriate salt concentration.

observation reflects the homogeneity of the adsorbed film at length scales above 10 nm.

Another characteristic effect of patch–charge heterogeneities can be observed in the fast aggregation regime near the charge neutralization point. Fig. 16a shows stability ratios *versus* salt concentration at the charge neutralization point for dendritic PAMAM of different molecular masses. One observes that the stability ratio decreases with decreasing salt concentration and that this effect becomes increasingly pronounced with increasing molecular mass. This trend can be interpreted with the increasing strength of the patch–charge interactions. Calculations of the stability ratio by including the non-DLVO patch–charge contribution given in eqn (19) capture the salt dependence rather well. Therefore, we interpret this enhancement as originating from patch–charge attractions. Due to their electrostatic nature, these interactions are screened at higher salt concentrations. Since these patches increase in size with increasing molecular mass, this effect also becomes more important under these conditions. Fig. 16b illustrates that this enhancement in the stability ratio at the charge neutralization point can be also observed for different linear PEs. This trend was reported for sulfate latex particles neutralized with PVA, BPEI, or poly(aminoethyl methacrylate)[49,56,143] or amidine particles with PSS or PAA.[140,148] Adsorbed LPEI layers do not show this enhancement due to their lateral homogeneity.[150]

The question to what extent bridging forces are relevant in the aggregation process of charged particles involving oppositely charged PEs still remains open. The observed trends in the available experimental data are qualitatively consistent with DLVO theory and patch–charge attractions. While the effect of patch–charge attractions can be modelled with an exponential force profile, this treatment is approximate due to inherent lateral heterogeneity of the surface. At this point, no quantitative theory is capable of predicting aggregation rate constants from the respective surface charge distributions. Direct force measurements discussed in Section 3 confirm that bridging events are rare at low salt concentrations, and under these conditions bridging forces will be unimportant. At higher salt concentrations, however, bridging events can be frequently

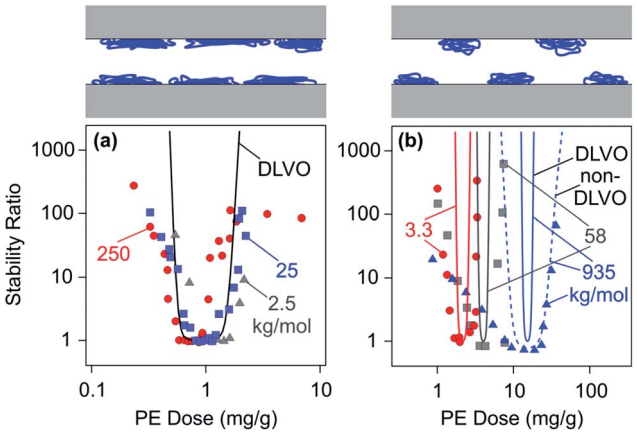

Fig. 15 Dependence of stability ratios of sulfate latex particles on the PE dose for different molecular masses in monovalent electrolyte solutions at pH 4.0 and comparison with DLVO theory. (a) LPEI in an electrolyte of 10 mM[150] and (b) dendritic PAMAM dendrimers at 1 mM.[155] The dashed line illustrates the effect of additional non-DLVO patch–charge attractions. The schemes on the top illustrate the homogeneous LPEI and heterogeneous PAMAM layers.

observed with the AFM, and therefore bridging forces could play a more important role. In this regime, however, the prevailing attractive interactions induce fast aggregation, and the corresponding rate depends only weakly on the strength of the attractive forces. In some systems, enhanced aggregation rates in the fast regime in the presence of alginate and multivalent cations were interpreted in terms of gelation, but they might also represent a signature of bridging.[236,237] However, analogous effects were not reported for other PEs so far.

Depletion destabilization. At higher polymer concentrations, typically around few g L^{-1}, neutral polymers were shown to destabilize colloidal suspensions through depletion forces.[208,238] A similar destabilization could be achieved by PEs and nano-sized charged particles having the same charge as the particles.[239–241] The addition of neutral polymers to suspensions of charged particles does initially enhance the aggregation processes, but leads to phase separation and gelation at later times.[208] Similar phenomena are expected in charged colloidal suspensions in the presence of higher concentrations of oppositely charged PEs, but we are unaware of any systematic studies of the aggregation phenomena in such systems.

5 Outlook

Polyelectrolytes (PEs) adsorb irreversibly to oppositely charged substrates until saturation, which results in thin monolayers, which have the opposite charge than the substrate. Due to the irreversible nature of the adsorption process, the addition of PEs to colloidal suspensions at smaller doses leads to the formation of unsaturated layers, and thereby charge reversal can be induced.

The principal forces acting between saturated layers are repulsive due to double layer forces and the corresponding particle suspensions are stable. For unsaturated layers near the charge reversal point, the interaction forces are attractive and the suspensions become unstable. Both phenomena are in agreement with DLVO theory, which can even describe interactions between homogeneous films quantitatively. For laterally heterogeneous films, attractive patch–charge interactions induce additional attractive forces leading to faster aggregation than predicted by DLVO theory.[47]

In spite of this reasonable level of understanding, we are still far away from being able to quantitatively predict interaction forces and colloidal stability solely from properties of the PEs and of the substrates. The charge reversal point for unsaturated layers can be estimated by assuming stoichiometric charge neutralization, even though numerous PEs adsorb in a super-stoichiometric way due to counterion co-adsorption.[31] However, a proper way to address the extent of this co-adsorption process is currently unknown. Similarly, there are a number of uncertainties as to how to reliably estimate electric surface potentials of surfaces with adsorbed PEs.

Better characterization of the lateral surface structure of PE-coated surfaces and of the resulting surface charge heterogeneities represents an important need to progress further. At this point, we have little knowledge concerning the type of surface charge heterogeneities, the respective length scales, and when such layers might be considered as homogeneous. Most promising are AFM imaging techniques,[134] but obtaining high-resolution maps of surface potentials represents a challenge. Such maps can be interpreted in terms of radial distribution functions, as recently carried out with computer simulation results,[41] but corresponding experimental results are only available for dendritic PAMAM.[34,133] We further lack reliable models to estimate the interaction forces involving heterogeneously charged surfaces. In particular, such models must go beyond the current simplistic regular lattice arrangements,[186,242] and the question of random, liquid-like structures must be addressed.

The relevance of forces that are well established for neutral polymers, such as steric repulsion, bridging attraction, and depletion interactions, should be revisited for PEs in more detail. Based on the above discussion, bridging forces appear irrelevant at low salt levels and for highly charged PEs. With

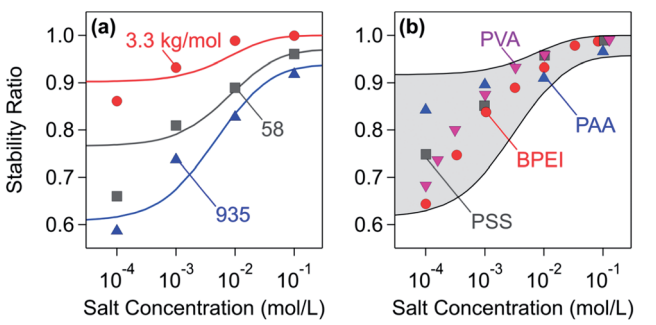

Fig. 16 The dependence of the stability ratios on the salt concentration at the charge neutralization point. Solid lines are calculations including non-DLVO contributions from patch–charge interactions. (a) Sulfate latex particles at pH 4.0 in the presence of dendritic PAMAM[155] and (b) amidine particles in the presence of linear PSS and PAA and sulfate latex in the presence of BPEI and PVA.[49,140,143,148]

increasing salt levels and decreasing charge densities, the PEs start to resemble neutral polymers, and thus steric and bridging forces will start to play a more important role.[109,178] However, it is unclear to us under what conditions this transition happens and what the respective mechanisms are.

On the other hand, depletion interactions have been established to play an important role at elevated PE concentrations. While depletion forces induced by non-adsorbing PEs have been studied in detail,[44,201] we have little information concerning such forces for PEs in the presence of oppositely charged substrates. An adsorbed saturated PE layer will make the surface effectively non-adsorbing for additional PE molecules, and thus the depletion interactions in these systems might well resemble the non-adsorbing case.

We hope that these questions will be addressed in the future by combining experimental techniques, computer simulations, and theory. These efforts are expected to lead to a more detailed picture of PE adsorption processes and the resulting interaction forces between substrates, and finally should give rise to reliable predictive tools that could be used to design optimal systems of PEs and substrates for the processes in question.

List of abbreviations

The corresponding structural formulae of all PEs discussed are given in Fig. 1.

AFM	Atomic force microscope
BPEI	Branched poly(ethylene imine)
CCC	Critical coagulation concentration
DLS	Dynamic light scattering
DLVO	Derjaguin, Landau, Verwey, and Overbeek
LPEI	Linear poly(ethylene imine)
PAA	Poly(acrylic acid)
PAMAM	Poly(amido amine)
PDDA	Poly(diallyldimethyl ammonium)
PE	Polyelectrolyte
PLL	Poly(L-lysine)
PSS	Poly(styrene sulfonate)
PVA	Poly(vinyl amine)
PVP	Poly(vinyl pyridine)
RSA	Random sequential adsorption
SFA	Surface forces apparatus
SCF	Self-consistent field.

Acknowledgements

We acknowledge useful discussions with Zbigniew Adamczyk, Vincent Ball, Lars Forsmann, Bo Jönsson, Christophe Labbez, Ger Koper, Robert Meszaros, Raffaele Mezzenga, Georg Papastavrou, Ionel Popa, Maria Santore, Imre Varga, and Corinne Vebert. We further thank Sergiy Minko for providing the high-resolution images appearing in Fig. 6c and d and Zbigniew Adamczyk for his permission to reproduce the data in Fig. 8d. This research was supported by the Swiss National Science Foundation, University of Geneva, State Secretariat for Education, Research and Innovation within the COST Action D43, and the EU Framework Program.

References

1 B. Bolto and J. Gregory, *Water Res.*, 2007, **41**, 2301–2324.
2 D. Horn and F. Linhart, *Retention aids*, Blackie Academic and Professional, London, 2nd edn, 1996.
3 N. Tobori and T. Amari, *Colloids Surf., A*, 2003, **215**, 163–171.
4 A. M. Howe, R. D. Wesley, M. Bertrand, M. Cote and J. Leroy, *Langmuir*, 2006, **22**, 4518–4525.
5 X. N. Chen, R. X. Huang and R. Pelton, *Ind. Eng. Chem. Res.*, 2005, **44**, 2078–2085.
6 I. Pochard, C. Labbez, A. Nonat, H. Vija and B. Jonsson, *Cem. Concr. Res.*, 2010, **40**, 1488–1494.
7 T. Phenrat, N. Saleh, K. Sirk, H. J. Kim, R. D. Tilton and G. V. Lowry, *J. Nanopart. Res.*, 2008, **10**, 795–814.
8 E. J. Bishop, D. E. Fowler, J. M. Skluzacek, E. Seibel and T. E. Mallouk, *Environ. Sci. Technol.*, 2010, **44**, 9069–9074.
9 S. Kim, J. H. So, D. J. Lee and S. M. Yang, *J. Colloid Interface Sci.*, 2008, **319**, 48–52.
10 E. Matijevic and S. V. Babu, *J. Colloid Interface Sci.*, 2008, **320**, 219–237.
11 A. S. Hoffman, *Adv. Drug Delivery Rev.*, 2012, **64**, 18–23.
12 V. Salgueirino-Maceira, F. Caruso and L. M. Liz-Marzan, *J. Phys. Chem. B*, 2003, **107**, 10990–10994.
13 S. Schwarz, J. E. Wong, J. Bornemann, M. Hodenius, U. Himmelreich, W. Richtering, M. Hoehn, M. Zenke and T. Hieronymus, *Nanomed. Nanotechnol. Biol. Med.*, 2012, **8**, 682–691.
14 R. Mezzenga, P. Schurtenberger, A. Burbidge and M. Michel, *Nat. Mater.*, 2005, **4**, 729–740.
15 G. Decher, *Science*, 1997, **277**, 1232–1237.
16 D. G. Shchukin, G. B. Sukhorukov and H. Möhwald, *Angew. Chem., Int. Ed.*, 2003, **42**, 4472–4475.
17 A. Fery, F. Dubreuil and H. Möhwald, *New J. Phys.*, 2004, **6**, 18.
18 T. Radeva and M. Grozeva, *J. Colloid Interface Sci.*, 2005, **287**, 415–421.
19 J. Ruhe, M. Ballauff, M. Biesalski, P. Dziezok, F. Grohn, D. Johannsmann, N. Houbenov, N. Hugenberg, R. Konradi, S. Minko, M. Motornov, R. R. Netz, M. Schmidt, C. Seidel, M. Stamm, T. Stephan, D. Usov and H. N. Zhang, *Adv. Polym. Sci.*, 2004, **165**, 79–150.
20 M. Ballauff and O. Borisov, *Curr. Opin. Colloid Interface Sci.*, 2006, **11**, 316–323.
21 S. Moya, O. Azzaroni, T. Farhan, V. L. Osborne and W. T. S. Huck, *Angew. Chem., Int. Ed.*, 2005, **44**, 4578–4581.
22 J. L. Dalsin, L. Lin, S. Tosatti, J. Voros, M. Textor and P. B. Messersmith, *Langmuir*, 2005, **21**, 640–646.
23 M. Elzbieciak-Wodka, M. Kolasinska-Sojka, D. Wodka, P. Nowak and P. Warszynski, *J. Electroanal. Chem.*, 2011, **661**, 162–170.
24 M. A. Cohen Stuart, W. T. S. Huck, J. Genzer, M. Muller, C. Ober, M. Stamm, G. B. Sukhorukov, I. Szleifer, V. V. Tsukruk, M. Urban, F. Winnik, S. Zauscher, I. Luzinov and S. Minko, *Nat. Mater.*, 2010, **9**, 101–113.

25 N. T. Qazvini, S. Bolisetty, J. Adamcik and R. Mezzenga, *Biomacromolecules*, 2012, **13**, 2136–2147.
26 N. G. Hoogeveen, M. A. Cohen Stuart and G. J. Fleer, *J. Colloid Interface Sci.*, 1996, **182**, 133–145.
27 N. G. Hoogeveen, M. A. Cohen Stuart and G. J. Fleer, *J. Colloid Interface Sci.*, 1996, **182**, 146–157.
28 M. Porus, P. Maroni and M. Borkovec, *Langmuir*, 2012, **28**, 5642–5651.
29 J. Blaakmeer, M. R. Bohmer, M. A. Cohen Stuart and G. J. Fleer, *Macromolecules*, 1990, **23**, 2301–2309.
30 R. Rehmet and E. Killmann, *Colloids Surf., A*, 1999, **149**, 323–328.
31 J. Kleimann, C. Gehin-Delval, H. Auweter and M. Borkovec, *Langmuir*, 2005, **21**, 3688–3698.
32 E. Seyrek, J. Hierrezuelo, A. Sadeghpour, I. Szilagyi and M. Borkovec, *Phys. Chem. Chem. Phys.*, 2011, **13**, 12716–12719.
33 Z. Adamczyk, K. Sadlej, E. Wajnryb, M. Nattich, M. L. Ekiel-Jezewska and J. Blawzdziewicz, *Adv. Colloid Interface Sci.*, 2010, **153**, 1–29.
34 B. P. Cahill, G. Papastavrou, G. J. M. Koper and M. Borkovec, *Langmuir*, 2008, **24**, 465–473.
35 G. J. Fleer, M. A. Cohen Stuart, J. M. H. M. Scheutjens, T. Cosgrove and B. Vincent, *Polymers at Interfaces*, Chapman and Hall, London, 1993.
36 C. Holm, J. F. Joanny, K. Kremer, R. R. Netz, P. Reineker, C. Seidel, T. A. Vilgis and R. G. Winkler, *Adv. Polym. Sci.*, 2004, **166**, 67–111.
37 R. R. Netz and D. Andelman, *Phys. Rep.*, 2003, **380**, 1–95.
38 A. V. Dobrynin, *Curr. Opin. Colloid Interface Sci.*, 2008, **13**, 376–388.
39 C. Y. Kong and M. Muthukumar, *J. Chem. Phys.*, 1998, **109**, 1522–1527.
40 J. Forsman, *Langmuir*, 2012, **28**, 5138–5150.
41 J. Y. Carrillo and A. V. Dobrynin, *Langmuir*, 2007, **23**, 2472–2482.
42 M. A. G. Dahlgren, A. Waltermo, E. Blomberg, P. M. Claesson, L. Sjostrom, T. Akesson and B. Jonsson, *J. Phys. Chem.*, 1993, **97**, 11769–11775.
43 P. M. Claesson, E. Poptoshev, E. Blomberg and A. Dedinaite, *Adv. Colloid Interface Sci.*, 2005, **114**, 173–187.
44 S. Biggs, D. C. Prieve and R. R. Dagastine, *Langmuir*, 2005, **21**, 5421–5428.
45 E. S. Pagac, R. D. Tilton and D. C. Prieve, *Langmuir*, 1998, **14**, 5106–5112.
46 X. C. Xing, G. Q. Sun, Z. F. Li and T. Ngai, *Langmuir*, 2012, **28**, 16022–16028.
47 I. Popa, G. Gillies, G. Papastavrou and M. Borkovec, *J. Phys. Chem. B*, 2009, **113**, 8458–8461.
48 M. Finessi, P. Sinha, I. Szilagyi, I. Popa, P. Maroni and M. Borkovec, *J. Phys. Chem. B*, 2011, **115**, 9098–9105.
49 F. Bouyer, A. Robben, W. L. Yu and M. Borkovec, *Langmuir*, 2001, **17**, 5225–5231.
50 M. Ashmore, J. Hearn and F. Karpowicz, *Langmuir*, 2001, **17**, 1069–1073.
51 Y. K. Leong, P. J. Scales, T. W. Healy and D. V. Boger, *Colloids Surf., A*, 1995, **95**, 43–52.
52 B. Derjaguin and L. D. Landau, *Acta Physicochim. URSS*, 1941, **14**, 633–662.
53 E. J. W. Verwey and J. T. G. Overbeek, *Theory of Stability of Lyophobic Colloids*, Elsevier, Amsterdam, 1948.
54 W. B. Russel, D. A. Saville and W. R. Schowalter, *Colloidal Dispersions*, Cambridge University Press, Cambridge, 1989.
55 V. K. La Mer and T. W. Healy, *Rev. Pure Appl. Chem.*, 1963, **13**, 112–133.
56 J. Gregory, *J. Colloid Interface Sci.*, 1973, **42**, 448–456.
57 G. Olanya, J. Iruthayaraj, E. Poptoshev, R. Makuska, A. Vareikis and P. M. Claesson, *Langmuir*, 2008, **24**, 5341–5349.
58 A. Naderi, G. Olanya, R. Makuska and P. M. Claesson, *J. Colloid Interface Sci.*, 2008, **323**, 223–228.
59 Y. Guo, J. van Beek, B. Zhang, M. Colussi, P. Walde, A. Zhang, M. Kröger, A. Halperin and A. D. Schlüter, *J. Am. Chem. Soc.*, 2009, **131**, 11841–11854.
60 J. J. Ramsden, *Chem. Soc. Rev.*, 1995, **24**, 73–78.
61 J. R. Lu, X. B. Zhao and M. Yaseen, *Curr. Opin. Colloid Interface Sci.*, 2007, **12**, 9–16.
62 Z. Adamczyk, *Curr. Opin. Colloid Interface Sci.*, 2012, **17**, 173–186.
63 V. Ball, A. Bentaleb, J. Hemmerle, J. C. Voegel and P. Schaaf, *Langmuir*, 1996, **12**, 1614–1621.
64 P. M. Claesson, E. Blomberg, J. C. Froberg, T. Nylander and T. Arnebrant, *Adv. Colloid Interface Sci.*, 1995, **57**, 161–227.
65 R. A. Silva, M. D. Urzua, D. F. S. Petri and P. L. Dubin, *Langmuir*, 2010, **26**, 14032–14038.
66 Z. Adamczyk, J. Barbasz and M. Ciesla, *Langmuir*, 2011, **27**, 6868–6878.
67 A. Mecke, I. Lee, J. R. Baker, M. M. B. Holl and B. G. Orr, *Eur. Phys. J. E*, 2004, **14**, 7–16.
68 S. Block and C. A. Helm, *Phys. Rev. E: Stat., Nonlinear, Soft Matter Phys.*, 2007, **76**, 030801.
69 L. Muresan, P. Maroni, I. Popa, M. Porus, R. Longtin, G. Papastavrou and M. Borkovec, *Macromolecules*, 2011, **44**, 5069–5071.
70 M. Porus, P. Maroni and M. Borkovec, *Langmuir*, 2012, **28**, 17506–17516.
71 Y. Samoshina, T. Nylander, V. Shubin, R. Bauer and K. Eskilsson, *Langmuir*, 2005, **21**, 5872–5881.
72 S. M. Notley, S. Biggs, V. S. J. Craig and L. Wagberg, *Phys. Chem. Chem. Phys.*, 2004, **6**, 2379–2386.
73 H. G. Pedersen and L. Bergstrom, *J. Am. Ceram. Soc.*, 1999, **82**, 1137–1145.
74 A. Gromer, M. Rawiso and M. Maaloum, *Langmuir*, 2008, **24**, 8950–8953.
75 T. Abraham, *Polymer*, 2002, **43**, 849–855.
76 J. Gregory and S. Barany, *Adv. Colloid Interface Sci.*, 2011, **169**, 1–12.
77 C. Porcel, P. Lavalle, V. Ball, G. Decher, B. Senger, J. C. Voegel and P. Schaaf, *Langmuir*, 2006, **22**, 4376–4383.
78 E. Laarz, A. Meurk, J. A. Yanez and L. Bergstrom, *J. Am. Ceram. Soc.*, 2001, **84**, 1675–1682.
79 A. P. Ngankam and P. R. Van Tassel, *Proc. Natl. Acad. Sci. U. S. A.*, 2007, **104**, 1140–1145.

80 J. Penfold, I. Tucker, R. K. Thomas, D. J. F. Taylor, X. L. Zhang, C. Bell, C. Breward and P. Howell, *Langmuir*, 2007, **23**, 3128–3136.
81 L. Muresan, P. Sinha, P. Maroni and M. Borkovec, *Colloids Surf., A*, 2011, **390**, 225–230.
82 H. Walter, C. Harrats, P. Muller-Buschbaum, R. Jerome and M. Stamm, *Langmuir*, 1999, **15**, 1260–1267.
83 Z. Adamczyk, M. Nattich and J. Barbasz, *Adv. Colloid Interface Sci.*, 2009, **147–148**, 2–17.
84 N. Kozlova and M. M. Santore, *Langmuir*, 2006, **22**, 1135–1142.
85 K. L. Chen and M. Elimelech, *Environ. Sci. Technol.*, 2008, **42**, 7607–7614.
86 S. Abalde-Cela, S. Ho, B. Rodriguez-Gonzalez, M. A. Correa-Duarte, R. A. Alvarez-Puebla, L. M. Liz-Marzan and N. A. Kotov, *Angew. Chem., Int. Ed.*, 2009, **48**, 5326–5329.
87 D. Sebok, T. Szabo and I. Dekany, *Appl. Surf. Sci.*, 2009, **255**, 6953–6962.
88 R. R. Netz and J. F. Joanny, *Macromolecules*, 1999, **32**, 9013–9025.
89 G. J. M. Koper and M. Borkovec, *Polymer*, 2010, **51**, 5649–5662.
90 N. Volk, D. Vollmer, M. Schmidt, W. Oppermann and K. Huber, *Adv. Polym. Sci.*, 2004, **166**, 29–65.
91 I. Popa, B. P. Cahill, P. Maroni, G. Papastavrou and M. Borkovec, *J. Colloid Interface Sci.*, 2007, **309**, 28–35.
92 N. P. Huang, R. Michel, J. Voros, M. Textor, R. Hofer, A. Rossi, D. L. Elbert, J. A. Hubbell and N. D. Spencer, *Langmuir*, 2001, **17**, 489–498.
93 Z. Adamczyk, A. Michna, M. Szaraniec, A. Bratek and J. Barbasz, *J. Colloid Interface Sci.*, 2007, **313**, 86–96.
94 I. Varga, A. Mezei, R. Meszaros and P. M. Claesson, *Soft Matter*, 2011, **7**, 10701–10712.
95 R. Longtin, P. Maroni and M. Borkovec, *Langmuir*, 2009, **25**, 2928–2934.
96 R. Kargl, T. Mohan, M. Bracic, M. Kulterer, A. Doliska, K. Stana-Kleinschek and V. Ribitsch, *Langmuir*, 2012, **28**, 11440–11447.
97 M. Jiang, I. Popa, P. Maroni and M. Borkovec, *Colloids Surf., A*, 2010, **360**, 20–25.
98 L. E. Enarsson and L. Wagberg, *Langmuir*, 2008, **24**, 7329–7337.
99 R. Meszaros, I. Varga and T. Gilanyi, *Langmuir*, 2004, **20**, 5026–5029.
100 R. C. van Duijvenbode, I. B. Rietveld and G. J. M. Koper, *Langmuir*, 2000, **16**, 7720–7725.
101 Z. Adamczyk, L. Szyk and P. Warszynski, *J. Colloid Interface Sci.*, 1999, **209**, 350–361.
102 H. Dautzenberg, E. Gornitz and W. Jaeger, *Macromol. Chem. Phys.*, 1998, **199**, 1561–1571.
103 Y. Tie, C. Calonder and P. R. Van Tassel, *J. Colloid Interface Sci.*, 2003, **268**, 1–11.
104 J. W. Evans, *Rev. Mod. Phys.*, 1993, **65**, 1281–1329.
105 Z. Adamczyk, B. Senger, J. C. Voegel and P. Schaaf, *J. Chem. Phys.*, 1999, **110**, 3118–3128.
106 B. Senger, J. C. Voegel and P. Schaaf, *Colloids Surf., A*, 2000, **165**, 255–285.
107 I. Popa, G. Papastavrou and M. Borkovec, *Phys. Chem. Chem. Phys.*, 2010, **12**, 4863–4871.
108 M. Finessi, PhD, University of Geneva, 2013.
109 L. J. Kirwan, P. Maroni, S. H. Behrens, G. Papastavrou and M. Borkovec, *J. Phys. Chem. B*, 2008, **112**, 14609–14619.
110 D. Bauer, H. Buchhammer, A. Fuchs, W. Jaeger, E. Killmann, K. Lunkwitz, R. Rehmet and S. Schwarz, *Colloids Surf., A*, 1999, **156**, 291–305.
111 M. R. Bohmer, W. H. A. Heesterbeek, A. Deratani and E. Renard, *Colloids Surf., A*, 1995, **99**, 53–64.
112 S. A. Sukhishvili and S. Granick, *J. Chem. Phys.*, 1998, **109**, 6861–6868.
113 K. Esumi and M. Goino, *Langmuir*, 1998, **14**, 4466–4470.
114 R. C. van Duijvenbode, G. J. M. Koper and M. R. Bohmer, *Langmuir*, 2000, **16**, 7713–7719.
115 T. Sennerfors, D. Solberg and F. Tiberg, *J. Colloid Interface Sci.*, 2002, **254**, 222–226.
116 T. J. Barnes, I. Ametov and C. A. Prestidge, *Langmuir*, 2008, **24**, 12398–12404.
117 V. Shubin, *J. Colloid Interface Sci.*, 1997, **191**, 372–377.
118 J. Lyklema and L. Deschenes, *Adv. Colloid Interface Sci.*, 2011, **168**, 135–148.
119 N. Hansupalak and M. M. Santore, *Langmuir*, 2003, **19**, 7423–7426.
120 D. Cakara, C. Chassagne, C. Gehin-Delval and M. Borkovec, *Colloids Surf., A*, 2007, **294**, 174–180.
121 E. Illes and E. Tombacz, *Colloids Surf., A*, 2003, **230**, 99–109.
122 B. Cabot, A. Deratani and A. Foissy, *Colloids Surf., A*, 1998, **139**, 287–297.
123 Z. Adamczyk and P. Warszynski, *Adv. Colloid Interface Sci.*, 1996, **63**, 41–149.
124 M. Semmler, E. K. Mann, J. Ricka and M. Borkovec, *Langmuir*, 1998, **14**, 5127–5132.
125 Z. Adamczyk, *Adv. Colloid Interface Sci.*, 2003, **100**, 267–347.
126 A. V. Dobrynin, A. Deshkovski and M. Rubinstein, *Macromolecules*, 2001, **34**, 3421–3436.
127 M. Muthukumar, *J. Chem. Phys.*, 1987, **86**, 7230–7235.
128 J. Hierrezuelo, I. Szilagyi, A. Vaccaro and M. Borkovec, *Macromolecules*, 2010, **43**, 9108–9116.
129 F. Hook, B. Kasemo, T. Nylander, C. Fant, K. Sott and H. Elwing, *Anal. Chem.*, 2001, **73**, 5796–5804.
130 A. Vaccaro, J. Hierrezuelo, M. Skarba, P. Galletto, J. Kleimann and M. Borkovec, *Langmuir*, 2009, **25**, 4864–4867.
131 I. Popa, G. Gillies, G. Papastavrou and M. Borkovec, *J. Phys. Chem. B*, 2010, **114**, 3170–3177.
132 Y. Roiter and S. Minko, *J. Phys. Chem. B*, 2007, **111**, 8597–8604.
133 R. Pericet-Camara, G. Papastavrou and M. Borkovec, *Langmuir*, 2004, **20**, 3264–3270.
134 S. Minko and Y. Roiter, *Curr. Opin. Colloid Interface Sci.*, 2005, **10**, 9–15.
135 L. J. Kirwan, G. Papastavrou, M. Borkovec and S. H. Behrens, *Nano Lett.*, 2004, **4**, 149–152.
136 F. Valle, M. Favre, P. de los Rios, A. Rosa and G. Dietler, *Phys. Rev. Lett.*, 2005, **95**, 158105.

137 H. G. M. van de Steeg, M. A. Cohen Stuart, A. de Keizer and B. H. Bijsterbosch, *Langmuir*, 1992, **8**, 2538–2546.
138 I. Borukhov, D. Andelman and H. Orland, *Macromolecules*, 1998, **31**, 1665–1671.
139 P. Linse, *Macromolecules*, 1996, **29**, 326–336.
140 G. Gillies, W. Lin and M. Borkovec, *J. Phys. Chem. B*, 2007, **111**, 8626–8633.
141 J. Hierrezuelo, A. Sadeghpour, I. Szilagyi, A. Vaccaro and M. Borkovec, *Langmuir*, 2010, **26**, 15109–15111.
142 J. Hierrezuelo, A. Vaccaro and M. Borkovec, *J. Colloid Interface Sci.*, 2010, **347**, 202–208.
143 W. L. Yu, F. Bouyer and M. Borkovec, *J. Colloid Interface Sci.*, 2001, **241**, 392–399.
144 E. Illes and E. Tombacz, *J. Colloid Interface Sci.*, 2006, **295**, 115–123.
145 S. Sennato, D. Truzzolillo, F. Bordi, F. Sciortino and C. Cametti, *Colloids Surf., A*, 2009, **343**, 34–42.
146 F. Quemeneur, M. Rinaudo, G. Maret and B. Pepin-Donat, *Soft Matter*, 2010, **6**, 4471–4481.
147 A. Feiler, P. Jenkins and J. Ralston, *Phys. Chem. Chem. Phys.*, 2000, **2**, 5678–5683.
148 A. Sadeghpour, E. Seyrek, I. Szilagyi, J. Hierrezuelo and M. Borkovec, *Langmuir*, 2011, **27**, 9270–9276.
149 I. Szilagyi, A. Sadeghpour and M. Borkovec, *Langmuir*, 2012, **28**, 6211–6215.
150 I. Szilagyi, D. Rosicka, J. Hierrezuelo and M. Borkovec, *J. Colloid Interface Sci.*, 2011, **360**, 580–585.
151 A. Mezei and R. Meszaros, *Langmuir*, 2006, **22**, 7148–7151.
152 Z. Adamczyk, A. Zembala and A. Michna, *J. Colloid Interface Sci.*, 2006, **303**, 353–364.
153 I. Popa, G. Papastavrou and M. Borkovec, *Macromolecules*, 2010, **43**, 1129–1136.
154 J. Dejeu, L. Buisson, M. C. Guth, C. Roidor, F. Membrey, D. Charraut and A. Foissy, *Colloids Surf., A*, 2006, **288**, 26–35.
155 W. Lin, P. Galletto and M. Borkovec, *Langmuir*, 2004, **20**, 7465–7473.
156 J. Sabin, C. Vazquez-Vazquez, G. Prieto, F. Bordi and F. Sarmiento, *Langmuir*, 2012, **28**, 10534–10542.
157 J. Israelachvili, *Intermolecular and Surface Forces*, Academic Press, London, 3rd edn, 2011.
158 S. H. Behrens and M. Borkovec, *J. Phys. Chem. B*, 1999, **103**, 2918–2928.
159 G. Toikka, R. A. Hayes and J. Ralston, *Langmuir*, 1996, **12**, 3783–3788.
160 C. Gutsche, U. F. Keyser, K. Kegler and F. Kremer, *Phys. Rev. E: Stat., Nonlinear, Soft Matter Phys.*, 2007, **76**, 031403.
161 P. G. Hartley, I. Larson and P. J. Scales, *Langmuir*, 1997, **13**, 2207–2214.
162 J. Israelachvili, *Intermolecular and Surface Forces*, Academic Press, London, 2nd edn, 1992.
163 P. Sinha, I. Szilagyi, F. J. Montes Ruiz-Cabello, P. Maroni and M. Borkovec, *J. Phys. Chem. Lett.*, 2013, **4**, 648–652.
164 R. M. Pashley, *J. Colloid Interface Sci.*, 1981, **83**, 531–546.
165 G. Toikka and R. A. Hayes, *J. Colloid Interface Sci.*, 1997, **191**, 102–109.
166 G. Vigil, Z. H. Xu, S. Steinberg and J. Israelachvili, *J. Colloid Interface Sci.*, 1994, **165**, 367–385.
167 P. F. Luckham and J. Klein, *J. Chem. Soc., Faraday Trans. 1*, 1984, **80**, 865–878.
168 P. Berndt, K. Kurihara and T. Kunitake, *Langmuir*, 1992, **8**, 2486–2490.
169 R. Pericet-Camara, G. Papastavrou, S. H. Behrens, C. A. Helm and M. Borkovec, *J. Colloid Interface Sci.*, 2006, **296**, 496–506.
170 E. Poptoshev and P. M. Claesson, *Langmuir*, 2002, **18**, 2590–2594.
171 E. Poptoshev, M. W. Rutland and P. M. Claesson, *Langmuir*, 2000, **16**, 1987–1992.
172 P. M. Claesson and B. W. Ninham, *Langmuir*, 1992, **8**, 1406–1412.
173 G. Maurdev, L. Meagher, J. Ennis and M. L. Gee, *Langmuir*, 2001, **34**, 4151–4158.
174 C. E. McNamee, M. Matsumoto, P. G. Hartley, P. Mulvaney, Y. Tsujii and M. Nakahara, *Langmuir*, 2001, **17**, 6220–6227.
175 A. Szucs, T. Haraszti, I. Dekany and J. H. Fendler, *J. Phys. Chem. B*, 2001, **105**, 10579–10587.
176 P. G. Hartley and P. J. Scales, *Langmuir*, 1998, **14**, 6948–6955.
177 V. Bosio, F. Dubreuil, G. Bogdanovic and A. Fery, *Colloids Surf., A*, 2004, **243**, 147–155.
178 T. Abraham, D. Christendat, Z. Xu, J. Masliyah, J. F. Gohy and R. Jerome, *AIChE J.*, 2004, **50**, 2613–2626.
179 R. Podgornik and M. Licer, *Curr. Opin. Colloid Interface Sci.*, 2006, **11**, 273–279.
180 H. H. Huang and E. Ruckenstein, *Langmuir*, 2012, **28**, 16300–16305.
181 M. Rief, F. Oesterhelt, B. Heymann and H. E. Gaub, *Science*, 1997, **275**, 1295–1297.
182 T. Hugel, M. Grosholz, H. Clausen-Schaumann, A. Pfau, H. Gaub and M. Seitz, *Macromolecules*, 2001, **34**, 1039–1047.
183 X. Chatellier, T. J. Senden, J. F. Joanny and J. M. di Meglio, *Europhys. Lett.*, 1998, **41**, 303–308.
184 G. Papastavrou, L. J. Kirwan and M. Borkovec, *Langmuir*, 2006, **22**, 10880–10884.
185 E. Poptoshev, M. W. Rutland and P. M. Claesson, *Langmuir*, 1999, **15**, 7789–7794.
186 S. J. Miklavic, D. Y. C. Chan, L. R. White and T. W. Healy, *J. Phys. Chem.*, 1994, **98**, 9022–9032.
187 P. Richmond, *J. Chem. Soc., Faraday Trans. 2*, 1975, **71**, 1154–1163.
188 I. Popa, G. Papastavrou, M. Borkovec, M. Trulsson and B. Jonsson, *Langmuir*, 2009, **25**, 12435–12438.
189 J. Swenson, M. V. Smalley and H. L. M. Hatharasinghe, *Phys. Rev. Lett.*, 1998, **81**, 5840–5843.
190 Y. Zhou, Y. Gan, E. J. Wanless, G. J. Jameson and G. V. Franks, *Langmuir*, 2008, **24**, 10920–10928.
191 I. Borukhov, D. Andelman and H. Orland, *J. Phys. Chem. B*, 1999, **103**, 5042–5057.
192 J. Forsman and S. Nordholm, *Langmuir*, 2012, **28**, 4069–4079.
193 M. Turesson, J. Forsman and T. Akesson, *Langmuir*, 2006, **22**, 5734–5741.

194 D. Truzzolillo, F. Bordi, F. Sciortino and S. Sennato, *J. Chem. Phys.*, 2010, **133**, 024901.
195 C. E. Woodward, T. Akesson and B. Jonsson, *J. Chem. Phys.*, 1994, **101**, 2569–2576.
196 A. Broukhno, B. Jonsson, T. Akesson and P. N. Vorontsov-Velyaminov, *J. Chem. Phys.*, 2000, **113**, 5493–5501.
197 R. Podgornik, P. Akesson and B. Jonsson, *J. Chem. Phys.*, 1995, **102**, 9423–9434.
198 R. Podgornik, *J. Chem. Phys.*, 2003, **118**, 11286–11296.
199 S. Biggs and T. W. Healy, *J. Chem. Soc., Faraday Trans.*, 1994, **90**, 3415–3421.
200 S. Biggs, J. L. Burns, Y. D. Yan, G. J. Jameson and P. Jenkins, *Langmuir*, 2000, **16**, 9242–9248.
201 A. Sharma, S. N. Tan and J. Y. Walz, *J. Colloid Interface Sci.*, 1997, **191**, 236–246.
202 A. J. Milling, *J. Phys. Chem.*, 1996, **100**, 8986–8993.
203 X. J. Gong and T. Ngai, *Langmuir*, 2013, **29**, 5974–5981.
204 D. Kleshchanok, R. Tuinier and P. R. Lang, *J. Phys.: Condens. Matter*, 2008, **20**, 073101.
205 Y. Zeng and R. von Klitzing, *Langmuir*, 2012, **28**, 6313–6321.
206 M. Elimelech, J. Gregory, X. Jia and R. A. Williams, *Particle Deposition and Aggregation: Measurement, Modeling, and Simulation*, Butterworth-Heinemann Ltd., Oxford, 1995.
207 P. Sandkuhler, M. Lattuada, H. Wu, J. Sefcik and M. Morbidelli, *Adv. Colloid Interface Sci.*, 2005, **113**, 65–83.
208 C. Gogelein, G. Nagele, J. Buitenhuis, R. Tuinier and J. K. G. Dhont, *J. Chem. Phys.*, 2009, **130**, 204905.
209 M. Lattuada, H. Wu and M. Morbidelli, *Langmuir*, 2004, **20**, 4355–4362.
210 K. Masschaele, J. Fransaer and J. Vermant, *Soft Matter*, 2011, **7**, 7717–7726.
211 E. P. Honig, G. J. Roebersen and P. H. Wiersema, *J. Colloid Interface Sci.*, 1971, **36**, 97–102.
212 S. H. Behrens, M. Borkovec and P. Schurtenberger, *Langmuir*, 1998, **14**, 1951–1954.
213 M. Kobayashi, M. Skarba, P. Galletto, D. Cakara and M. Borkovec, *J. Colloid Interface Sci.*, 2005, **292**, 139–147.
214 M. Schudel, S. H. Behrens, H. Holthoff, R. Kretzschmar and M. Borkovec, *J. Colloid Interface Sci.*, 1997, **196**, 241–253.
215 H. Holthoff, S. U. Egelhaaf, M. Borkovec, P. Schurtenberger and H. Sticher, *Langmuir*, 1996, **12**, 5541–5549.
216 W. Lin, M. Kobayashi, M. Skarba, C. Mu, P. Galletto and M. Borkovec, *Langmuir*, 2006, **22**, 1038–1047.
217 H. Holthoff, A. Schmitt, A. Fernandez-Barbero, M. Borkovec, M. A. Cabrerizo-Vilchez, P. Schurtenberger and R. Hidalgo-Alvarez, *J. Colloid Interface Sci.*, 1997, **192**, 463–470.
218 S. H. Xu and Z. W. Sun, *Soft Matter*, 2011, **7**, 11298–11308.
219 D. R. E. Snoswell, J. M. Duan, D. Fornasiero and J. Ralston, *J. Colloid Interface Sci.*, 2005, **286**, 526–535.
220 H. Kihira, N. Ryde and E. Matijevic, *J. Chem. Soc., Faraday Trans.*, 1992, **88**, 2379–2386.
221 M. B. Einarson and J. C. Berg, *J. Colloid Interface Sci.*, 1993, **155**, 165–172.
222 C. Schneider, M. Hanisch, B. Wedel, A. Jusufi and M. Ballauff, *J. Colloid Interface Sci.*, 2011, **358**, 62–67.
223 S. H. Behrens, D. I. Christl, R. Emmerzael, P. Schurtenberger and M. Borkovec, *Langmuir*, 2000, **16**, 2566–2575.
224 T. Hiemstra and W. H. van Riemsdijk, *Langmuir*, 1999, **15**, 8045–8051.
225 S. Y. Shulepov and G. Frens, *J. Colloid Interface Sci.*, 1996, **182**, 388–394.
226 J. D. Feick and D. Velegol, *Langmuir*, 2002, **18**, 3454–3458.
227 K. L. Chen, S. E. Mylon and M. Elimelech, *Environ. Sci. Technol.*, 2006, **40**, 1516–1523.
228 G. Fritz, V. Schadler, N. Willenbacher and N. J. Wagner, *Langmuir*, 2002, **18**, 6381–6390.
229 X. Guo and M. Ballauff, *Langmuir*, 2000, **16**, 8719–8726.
230 C. N. Likos, K. A. Vaynberg, H. Lowen and N. J. Wagner, *Langmuir*, 2000, **16**, 4100–4108.
231 R. G. Smits, G. J. M. Koper and M. Mandel, *J. Phys. Chem.*, 1993, **97**, 5745–5751.
232 H. W. Walker and S. B. Grant, *Colloids Surf., A*, 1996, **119**, 229–239.
233 M. Trulsson, J. Forsman, T. Akesson and B. Jonsson, *Langmuir*, 2009, **25**, 6106–6112.
234 S. Schwarz, K. Lunkwitz, B. Kessler, U. Spiegler, E. Killmann and W. Jaeger, *Colloids Surf., A*, 2000, **163**, 17–27.
235 S. Schwarz, W. Jaeger, B. R. Paulke, S. Bratskaya, N. Smolka and J. Bohrisch, *J. Phys. Chem. B*, 2007, **111**, 8649–8654.
236 T. Abe, S. Kobayashi and M. Kobayashi, *Colloids Surf., A*, 2011, **379**, 21–26.
237 K. L. Chen, S. E. Mylon and M. Elimelech, *Langmuir*, 2007, **23**, 5920–5928.
238 J. E. Seebergh and J. C. Berg, *Langmuir*, 1994, **10**, 454–463.
239 A. Sharma, S. N. Tan and J. Y. Walz, *J. Colloid Interface Sci.*, 1997, **190**, 392–407.
240 M. J. Snowden, S. M. Clegg, P. A. Williams and I. D. Robb, *J. Chem. Soc., Faraday Trans.*, 1991, **87**, 2201–2207.
241 S. Rawson, K. Ryan and B. Vincent, *Colloids Surf.*, 1988, **34**, 89–93.
242 P. Richmond, *J. Chem. Soc., Faraday Trans. 2*, 1974, **70**, 1066–1073.